

Design, Synthesis, and Cytotoxicity of New Oxindole Sulfonamide Derivatives as Bruton's Tyrosine Kinase Inhibitors

Chandra Prakash Koraboina, Venkatanarayana Chowdary Maddipati, Narendran Annadurai, Soňa Gurská, Petr Džubák, Marián Hajdúch, Viswanath Das*, Rambabu Gundla*

ABSTRACT

As a regulator of the dual function of apoptosis in B cells, Bruton's tyrosine kinase (BTK) was the first discovered tyrosine kinase. It continues to draw interest as a potential therapy for autoimmune disorders, inflammation, and malignancies connected to B cells. The pathogenic alterations in various cancer tissues depend on mutant BTK for cell proliferation and survival, and BTK is also overexpressed in a range of hematopoietic cells. Due to this, BTK is emerging as a potential drug target to treat various human diseases, and several reversible and irreversible inhibitors have been developed and are being developed. As a result, BTK inhibition, clinically validated as an anticancer treatment, is finding great interest in B-cell malignancies and solid tumours. This study focuses on the design and synthesis of new oxindole sulfonamide derivatives as promising inhibitors of BTK with negligible off-target effects. The most cytotoxic compounds with greater basicity were PID-4 ($2.29 \pm 0.52 \mu\text{M}$), PID-6 ($9.37 \pm 2.47 \mu\text{M}$), and PID-19 ($2.64 \pm 0.88 \mu\text{M}$). These compounds caused a selective inhibition of Burkitt's lymphoma RAMOS cells without significant cytotoxicity in non-BTK cancerous and non-cancerous cell lines. Further, PID-4 showed promising activity in inhibiting BTK and downstream signalling cascades. As a potent inhibitor of Burkitt's lymphoma cells, PID-4 is a promising lead for developing novel chemotherapeutics.

KEYWORDS

Anticancer drug; Bruton's tyrosine kinase; B-cell malignancies; Knoevenagel condensation; Oxindole Sulfonamide

INTRODUCTION

Bruton's tyrosine kinase (BTK) is a Tec family kinase that functions as a nonreceptor tyrosine kinase.^{1,2} Tec family kinases (TFKs) form the second largest family of cytoplasmic tyrosine kinases in mammalian cells. BTK is critical for B-cell development, differentiation, and signalling.^{1,2} Moreover, BTK expression is assumed to be a prerequisite for B-cell proliferation and survival, and BTK-deficient B lymphocytes fail to reach the mature state and undergo premature death.³ The *BTK* gene comprises 19 exons and spans approximately 37.5 kb on the human X chromosome.⁴

With an estimated 19.3 million new diagnoses and 10 million deaths worldwide, cancer is one of the leading causes of human deaths as of 2020.⁵ The current anticancer drugs each have a different mode of action, ultimately leading to variations in how they affect different cancer types and healthy cells.⁶ A significant and practical worry with cancer is the development of resistance to current multi-drug chemotherapy and its poor pace of cure, severe side effects, and the overarching adverse impact on the lives of both patients and caregivers.^{6,7} Therefore, developing better and more effective chemotherapeutic drugs with minimal off-target effects is crucial for treating cancer.⁸

Angiogenesis, evasion of the anti-tumour immune system response, changes in cellular proliferation, survivability, motility, metabolism, and abnormal protein kinase activity are all critical characteristics of malignancies.⁹ BTK is an essential kinase for oncogenic signalling and plays a vital role in leukemic cell survival and is associated with different B-cell malignancies such as chronic lymphocytic leukaemia, mantle cell lymphoma (MCL), Waldenström's macroglobulinemia, and Follicular lymphoma.¹⁰⁻¹⁴ BTK was previously found to be mutated in X-linked agammaglobulinemia (XLA) and also found to be crucial for the development of B lymphocyte development.^{15,16} XLA is an immunodeficiency disorder that is inherited and was previously first described by Ogdon Bruton in 1952 and later reported through various research on recurrent bacterial infections. Due to a severe obstruction to B-cell growth in the bone marrow, the patients with XLA have low B cells circulating in their bodies, and the antibody count is nearly negligible in their serum.¹⁷

BTK has drawn much attention as a molecular target in medicinal chemistry since preclinical

and clinical investigations using small-molecule inhibitors have demonstrated outstanding anti-tumour effects.¹⁸ BTK inhibitors (BTKIs) may be divided into two categories depending on how they bind to BTK, their scaffold designs, and their mechanisms of action. The first category of irreversible inhibitors forms a covalent link with the ATP-binding site of BTK that has the amino acid residue Cys481. The other category of BTKIs consists of reversible inhibitors, which bind to an inactive version of the kinase by accessing the SH3 pocket of BTK.^{19–21}

In 2013, a significant milestone was achieved when ibrutinib, the first covalent and irreversible BTKI, received approval from the US Food and Drug Administration for treating relapsed and refractory MCL.²² Building on this success, the subsequent years witnessed the development and approval of second- and third-generation irreversible BTKIs, such as acalabrutinib, zanubrutinib, tirabrutinib, and orelabrutinib. These newer agents aimed to reduce the adverse effects of ibrutinib while broadening their application to various B-cell malignancies.²² Simultaneously, BTKIs have seen a surge in research and development, with several irreversible BTKIs currently in various phases of preclinical and clinical trials.¹⁸ While all five currently approved BTKIs are irreversible in their mode of action, there is a growing interest in exploring reversible inhibitors for treating haematological malignancies and autoimmune diseases.¹⁸ This ongoing exploration of different inhibition mechanisms underscores the dynamic nature of BTK research and its potential for therapeutic innovation. Against this backdrop, the quest for novel BTKIs continues to be an exciting and evolving area within medicinal chemistry. In this context, we report the design, synthesis, and biological evaluation of a series of novel oxindole sulfonamide derivatives as promising anti-BTK candidates.

RESULT AND DISCUSSION

Within drug discovery, there is a growing interest in harnessing the potential of hybridized bioactive molecules to create novel compounds that surpass the effectiveness of existing options. This approach promises to enhance therapeutic outcomes and mitigate adverse effects associated with current treatments (Figure 1). Among the key players in this endeavour, oxindole sulfonamide has emerged as a pivotal building block, providing a versatile scaffold for developing hybrid candidates with superior efficacy and improved safety profiles. Our research represents a multifaceted exploration into the fusion of bioactive molecules, with a particular

focus on oxindole sulfonamide. By coupling this scaffold with Tetrahydro Pyran, we sought to create hybrid compounds with enhanced anticancer properties against BTK-positive cancers. We rigorously evaluated the resultant hybrid compounds for their *in vitro* anticancer activity. In parallel with our experimental endeavours, we delved into the molecular aspects of these hybrid compounds through comprehensive molecular docking investigations. This computational approach allowed us to gain valuable insights into the interactions between our synthesized hybrids and their intended molecular targets. We aimed to elucidate these compounds' binding affinities and modes through molecular docking, shedding light on the mechanisms underlying their potential anticancer activity.

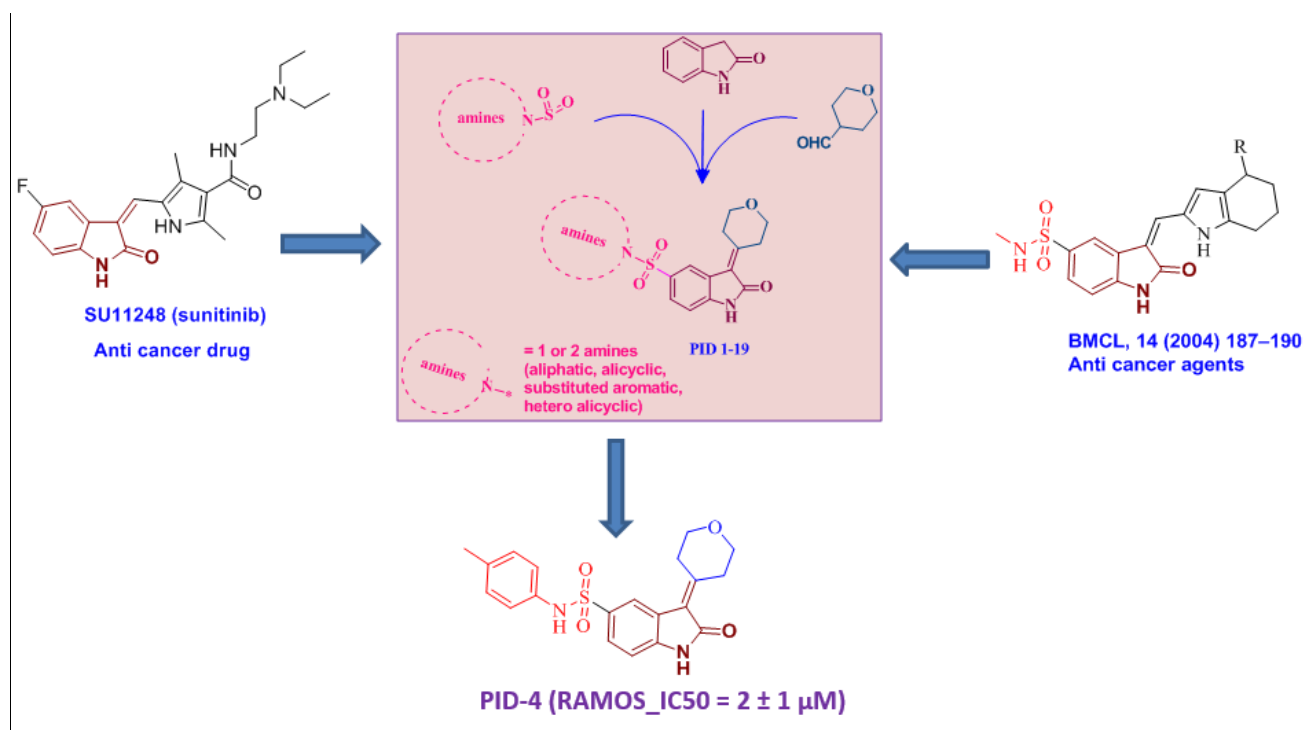
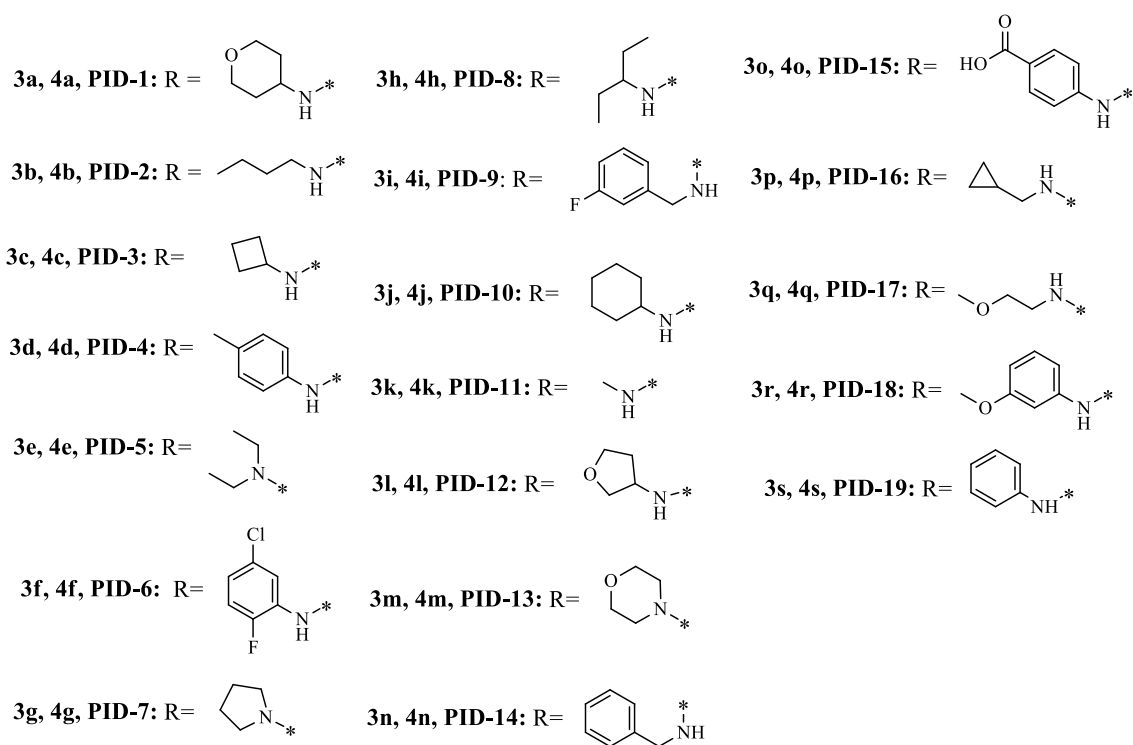
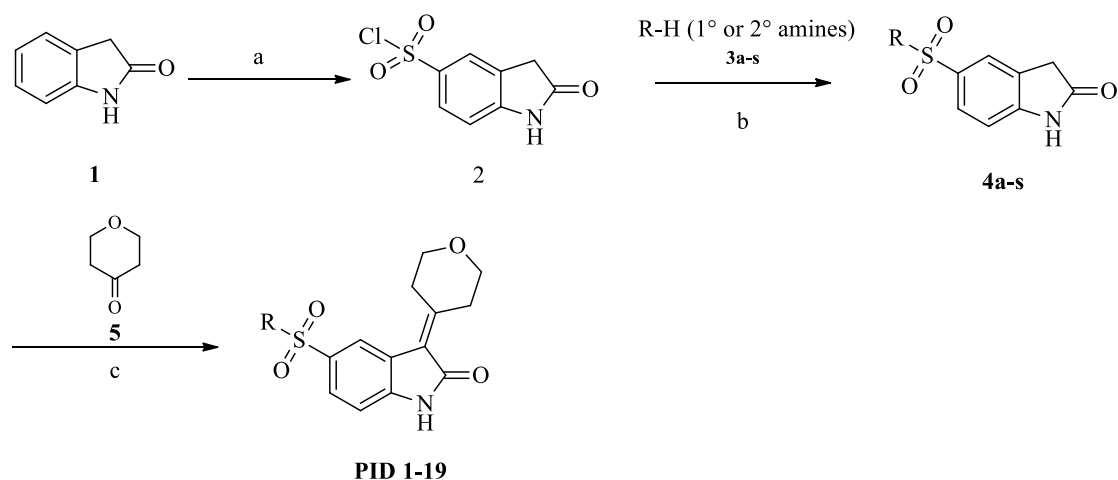


Figure 1. Designing of new oxindole sulfonamide derivatives as BTKI.

Chemistry

The general strategy for the synthesis of 3-(dihydro-2*H*-pyran-4(3*H*)-ylidene)-2-oxindoline-5-sulfonamide analogues (**PID 1-19**) was described in Scheme 1. Firstly, the commercially available indolin-2-one (**1**) was treated with chlorosulfonic acid at 70 °C to yield key

intermediate 2-oxoindoline-5-sulfonyl chloride (**2**) in 80%. It was observed that the sulfonyl chloride intermediate was slowly degraded to sulfonic acid on a long stand, which was consumed in below 30 days for the sulfonamide's formation. Different types of amines (**3a-s**) were used for the conversion of this sulfonyl chloride intermediate (**2**) to corresponding sulfonamide (**4a-s**) using pyridine as a base in 1,4-dioxane at ambient temperature, which proceeded for the next step without purification. Finally, we synthesized 3-(dihydro-2*H*-pyran-4(3*H*)-ylidene)-2-oxoindoline-5-sulfonamide analogues (**PID 1-19**) by Knoevenagel condensation of dihydro-2*H*-pyran-4(3*H*)-one (**5**) in the presence of pyrrolidine with corresponding sulfonamides (**4a-s**) in good yields. The Knoevenagel condensation gave better yields at room temperature instead of heating at reflux temperature. These synthesized targets were purified by flash column chromatography and characterized by spectroscopic methods. ¹H NMR, ¹³C NMR, HRMS, HPLC, and FT-IR spectra of all compounds are provided as Supporting Information.



Scheme 1. Reagents and conditions: (a) ClSO_3H , 70 °C, 1 h (b) amines **3a-s**, pyridine, 1,4-dioxane, rt, 2 h (c) dihydro-2*H*-pyran-4(3*H*)-one, pyrrolidine, ethanol, rt, 3 h.

Docking

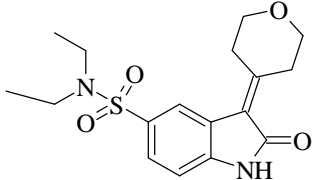
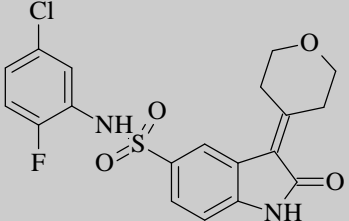
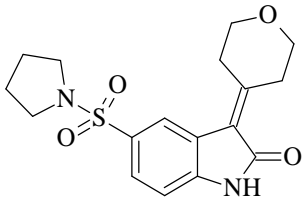
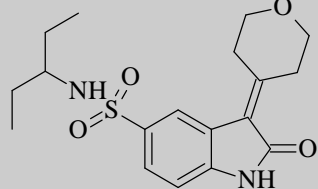
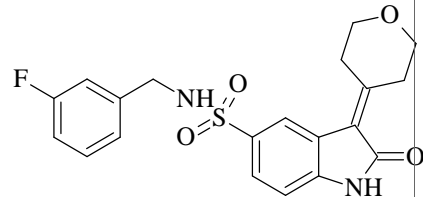
A docking study was conducted to gain insights into oxindole sulfonamide derivatives' binding affinity and intermolecular interactions with BTK. BTK complexed with an inhibitor ibrutinib (PDB ID- 5P9J), was used for docking analysis. Ibrutinib was used as a standard drug to screen

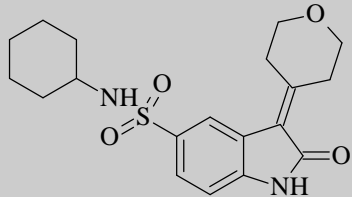
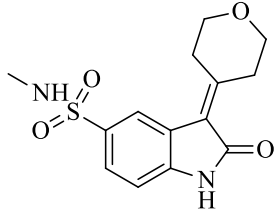
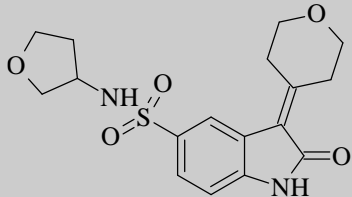
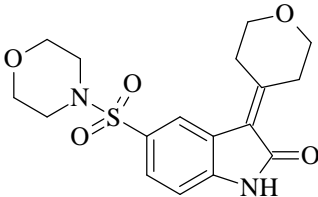
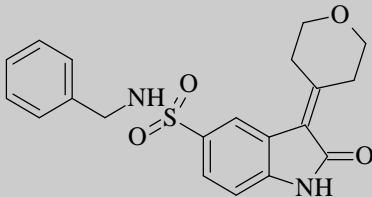
oxindole sulfonamide derivatives. Crystallographic data shows that ibrutinib and zanubrutinib share similar bioactive conformations within the wild-type BTK binding site.^{23,24} From these complexes, it was observed that besides the covalent bond with Cys481, the two complexes were mainly stabilized by similar interactions. This includes the cation- π contact between the phenoxyphenyl ring and Lys430 side chain and the hydrogen bonds with Met477 and Glu475 backbones. Noncovalent inhibitors that do not interact with Cys481 can inhibit C481R, T474I and T474M mutants and represent an attractive therapeutic option.²⁵ Noncovalent BTKIs provide several advantages over existing covalent inhibitors. Though covalent inhibitors lose potency against Cys481 mutants, some noncovalent inhibitors retain potent inhibition against C481S and C481R BTK mutants. This provides a probably practical treatment choice for ibrutinib-resistant or naïve patients.²⁵

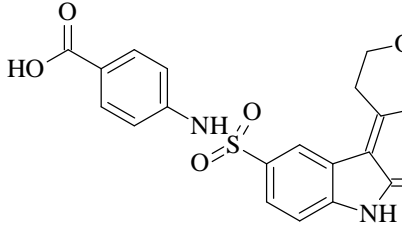
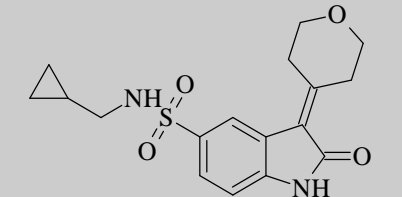
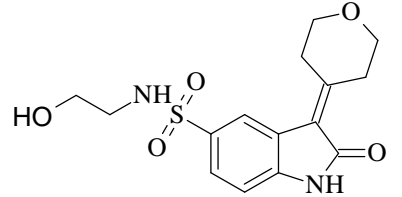
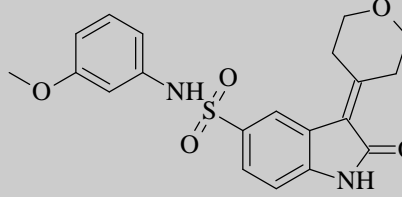
We docked all 19 oxindole sulfonamide derivatives into the binding site of BTK. The top 19 compounds were selected based on binding energy score. The molecular docking results include docking binding energy, the interacting amino acid residues in the binding pocket of the protein, and the type of interaction and structure of ligands (Table 1). Binding energies and molecular interactions of oxindole sulfonamide derivatives were compared with those of ibrutinib to select molecules for further studies. Ibrutinib exhibited the highest binding energy to the active site residues of BTK -10.8 kcal/mol and formed hydrogen bonds with Met 377, Glu375, Pi-cation stacking with Lys 430, Pi-anion stacking with Asp 539 and Pi-Alkyl Bond with Val416, which are found essential for interactions in the crystallographic complex. Compared to ibrutinib, all derivatives exhibited binding energy ranging from -7.9 to -10.8 kcal/mol. In particular, **PID-6** exhibited similar binding energy (dock score -10.8 kcal/mol) to the active site residues of BTK as ibrutinib. The docking scores of **PID-4** and **PID-19**, two other derivatives with better cytotoxicity in BTK-positive cells (see results in subsequent sections), were -10.3 kcal/mol and -10.7 kcal/mol, respectively. Molecular docking interactions of **PID-4**, **PID-6** and **PID-19** are shown in Figures 2-4. We selected the top 19 compounds with binding energy ranging from -7.9 to -10.8 kcal/mol, and showing interactions essential for inhibiting BTK were selected for further cytotoxicity profiling.

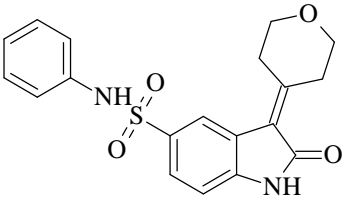
Table 1. Molecular Docking analysis results using Autodock Vina for all oxindole sulfonamide derivatives

Compound	Btk docking score	Structure	Amino acid interactions
PID-1	-10.3		Gly:409, Ser:538, Thr:474, Val:458, Met:449, ASP:539, Leu:542, Glu:475, Tyr:476, Ala:478 – Van der Waals; Gly:480 – Carbon Hydrogen Bond; Lys:430, Met:477 – Conventional Hydrogen Bond; Ala:428, Val:416, Ile:472 – Pi-Alkyl Bond; Leu:528, Leu: 408 – Pi-Sigma.
PID-2	-9.3		Glu:475, Tyr:476, Thr:474, Asp:539, Gly:409 – Van der Waals; Gly:480 – Carbon Hydrogen Bond; Met:477, Ser:538, Lys:430 – Conventional Hydrogen Bond; Ala:428, Val:416 – Pi-Alkyl Bond; Leu:408, Val:458, Phe:540, Leu:460 – Alkyl Bond; Leu:528 – Pi-Sigma.
PID-3	-10.0		Ala:478, Tyr:476, Glu:475, Thr:474, Leu:542, Asp:539, Ser:538, Val:458, Gly:409 – Van der Waals; Gly:480 – Carbon Hydrogen Bond; Lys:430, Met:477 – Conventional Hydrogen Bond; Ala:428, Val:416 – Pi-Alkyl Bond; Ile:472 – Alkyl Bond; Leu:528, Leu:408 – Pi-Sigma.
PID-4	-10.4		Phe:442, Val:458, Gly:411, GLN:412, Arg:525, Cys:527, Ser:538, Ala:428, Glu:475, Leu:460, Phe:442 – Van der Waals; Thr:474, Asn:526 – Conventional hydrogen Bond; Ile:472, Val:416 -Pi-Alkyl Bond; Leu:542, Lys:430, Met:449 – Alkyl bond; Leu:528 – Pi-Sigma.

PID-5	-8.8		Gly:411, Thr:474, Glu:475, Tyr:476, Cys:481, Ser:538, Asn:526, Asp:539 – Van der Waals; Leu:408, Gly:480, Arg:525 – Carbon Hydrogen Bond; Lys:430, Met:477 – Conventional hydrogen Bond; Val:416 – Pi-Alkyl Bond; Ala:428 – Alkyl Bond; Asp:539 – Pi-Anion; Leu:528 – Pi-Sigma.
PID-6	-10.8		Gly:409, Cys:481, Gly:480, Tyr:476, Glu:475, Met:449, Phe:442 – Van der Waal; Lys:430, Ser:538 – Conventional Hydrogen Bond; Val:416, Val:458, Ile:472, Ala:428 – Pi-Alkyl Bond; Leu:52 – Alkyl; Asp:539 – Pi-Anion; Leu:408, Leu:528, Thr:474 – Pi-Sigma.
PID-7	-9.6		Arg:525, Asn:526, Gly:411, Thr:474, Glu:475, Tyr:476 – Van der Waals; Asp:539, Gly:480, Leu:408 – Carbon Hydrogen Bond; Lys:430, Met:477 – Conventional hydrogen Bond; Ala:428 – Alkyl Bond; Leu:528, Val:416 – Pi-Sigma.
PID-8	-8.5		Asp:539, Cys:481, Gly:480 – Van der Waal; Met:477 – Carbon Hydrogen Bond; Lys:430 – Conventional Hydrogen Bond Ala:428, Leu:528, Leu:408 – Pi-Alkyl Bond; Val:416 – Pi-Sigma.
PID-9	-10.7		Phe:540, Met:449, Ser:538, Met:477, Cys:481, Gly:409, Thr:410, Gly:411, Val:458 – Van der Waals; Thr:474, Gly:480 – Carbon hydrogen Bond; Lys:430 – Conventional hydrogen Bond; Ile:472, Leu:542, Ala:428, Val:416, Ala:428 – Pi-Alkyl Bond; Leu:408 – Alkyl Bond; Asp:539 – Pi-Anion; Leu:528 – Pi-Sigma.

PID-10	-10.6		Cys:481, Gly:480, Tyr:476, Met:477, Val:458, Thr:474, Me:449, Ile:472, Sera:538, Leu:542, Lys:430 – Van der Waals; Asp:539 – Conventional Hydrogen Bond; Val:416, Leu:460, Phe:540, Ala:428, Leu:408 – Pi-Alkyl Bond; Leu:528 – Pi-Sigma.
PID-11	-7.9		Asp:539, Val:458, Gly:409, Cys:481, Ala:478, Tyr:476, Glu:475, Thr:474 – Van der Waals; Gly:480 – Carbon Hydrogen Bond; SER:538, Ls:430, Met:477 – Conventional Hydrogen Bond; Ala:428, Val:416 – Pi-Alkyl Bond; Leu:528, Leu:408 – Pi-Sigma.
PID-12	-9.3		Gly:411, Thr:410, Gly:409, Cys:481, Gly:480, Ala:478, Tyr:476, Glu:475, Thr:474, Val:458, Ser:538, Lys:430, Val:416 – Van der Waals; Leu:408, Met:477 – Conventional Hydrogen Bond; Ala:428, Leu:528 – Alkyl Bond.
PID-13	-9.6		Thr:410, Gly:409, Cys:481, Lys:430, Val:458, Thr:474, Glu:475, Tyr:476, Ala:478, Gly:480 – Van der Waals; Met:477 – Conventional hydrogen Bond; Val:416 – Pi-Alkyl Bond; Ala:428, Leu:528 – Alkyl Bond; Leu:408 – Pi-Sigma.
PID-14	-10.4		Met:449, Leu:542, Val:458, Ser:538, Glu:475, Tyr:476, Cys:481, Gly:409 – Van der Waals; Gly:480, Asp:539, Leu:408 – Carbon Hydrogen Bond; Met:477, Lys:430 – Conventional hydrogen Bond; Phe:540 – Amide Pi-Stacked; Leu:460, Ile:472, Ala:428, Val:416 – Pi-Alkyl; Leu:528, Thr:474 – Pi-Sigma.

<p>PID-15</p>	<p>-10.0</p>		<p>Ala:478, Tyr:476, Glu:475, Thr:474, Val:458, Ser:538, Phe:413, Asn:526, Gly:409, Cys:481, Thr:410, Gly:480 – Van der Waals; Met:477, Gln:412, Asp:539, Lys:430 – Conventional Hydrogen Bond; Gly:411 – Carbon Hydrogen Bond; Val:416 – Pi-Alkyl Bond; Ala:428, Leu:528 – Alkyl Bond; Leu:408 – Pi-Sigma.</p>
<p>PID-16</p>	<p>-9.8</p>		<p>Gly:409, Ser:538, Val:458, Leu:460, Thr:474, Glu:475, Tyr:476, Ala:478 – Van der Waals; Asp:539, Gly:480 – Carbon hydrogen Bond; Met:477, Lys:430 – Conventional hydrogen Bond; Ala:428, Val:416 – Pi-Alkyl Bond; Leu:542, Ile:472 – Alkyl Bond; Leu:528, Leu:408 – P-Sigma.</p>
<p>PID-17</p>	<p>-9.0</p>		<p>Gly:409, Val:458, Leu:542, Phe:540, Thr:474, Glu:475, Tyr:476, Ala:478 – Van der Waals; Ser:538, Met:477, Lys:430, Asp:539 – Conventional Hydrogen Bond; Gly:480 – Carbon Hydrogen Bond; Ala:428, Val:416 – Pi-Alkyl Bond; Leu:528, Leu:408 – Pi-Sigma.</p>
<p>PID-18</p>	<p>-9.9</p>		<p>Asp:539, Ser:538, Gly:480 – Van der Waals; Lys:430, Met:477 – Conventional Hydrogen Bond; Val:416 – Pi-Alkyl Bond; Leu:528, Ala:428 – Alkyl Bond; Leu:408 – Pi-Sigma.</p>

PID-19	-10.7		Cys:481, Gly:480, Met:477, Lys:430, Ser:538 – Van der Waals; Asp:539 – Conventional hydrogen Bond; Ala:428, Leu:408, Val:416 – Pi-Alkyl Bond; Leu:528 – Pi-Sigma.
---------------	-------	--	---

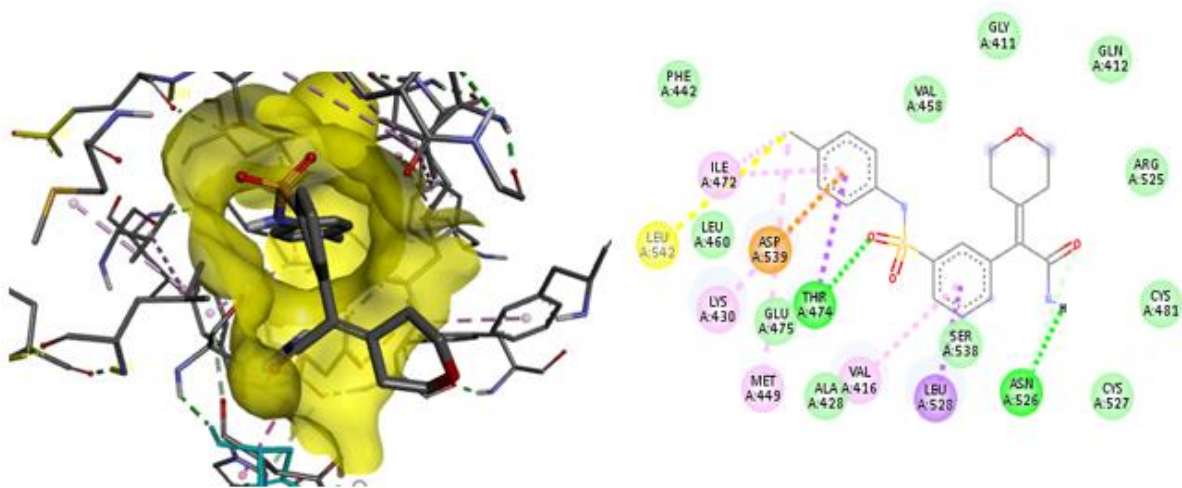


Figure 2. Molecular docking interaction of **PID-4** with BTK complexed with ibrutinib (PDB ID-5P9J).

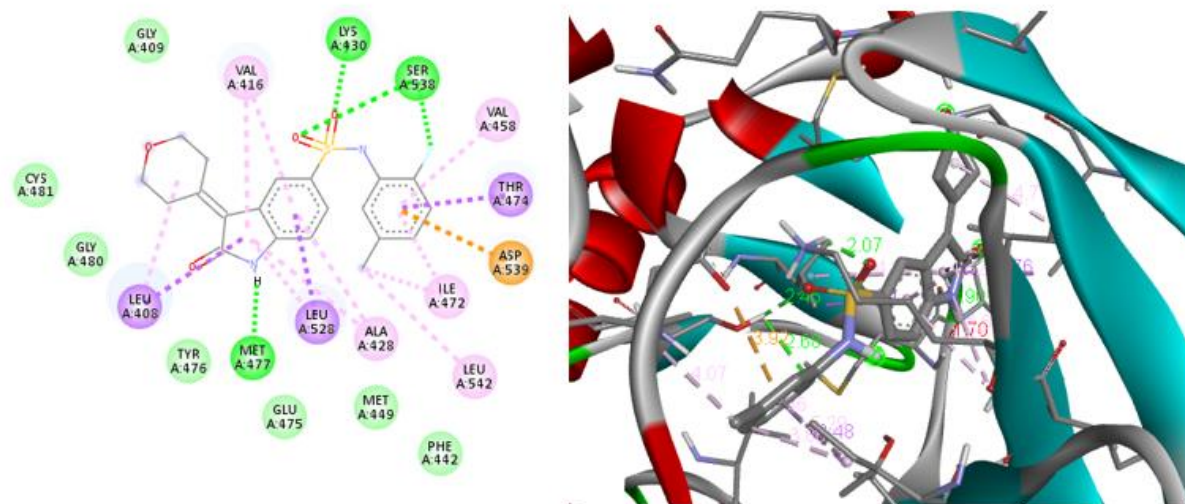


Figure 3. Molecular docking interaction of **PID-6** with BTK complexed with ibrutinib (PDB ID-5P9J).

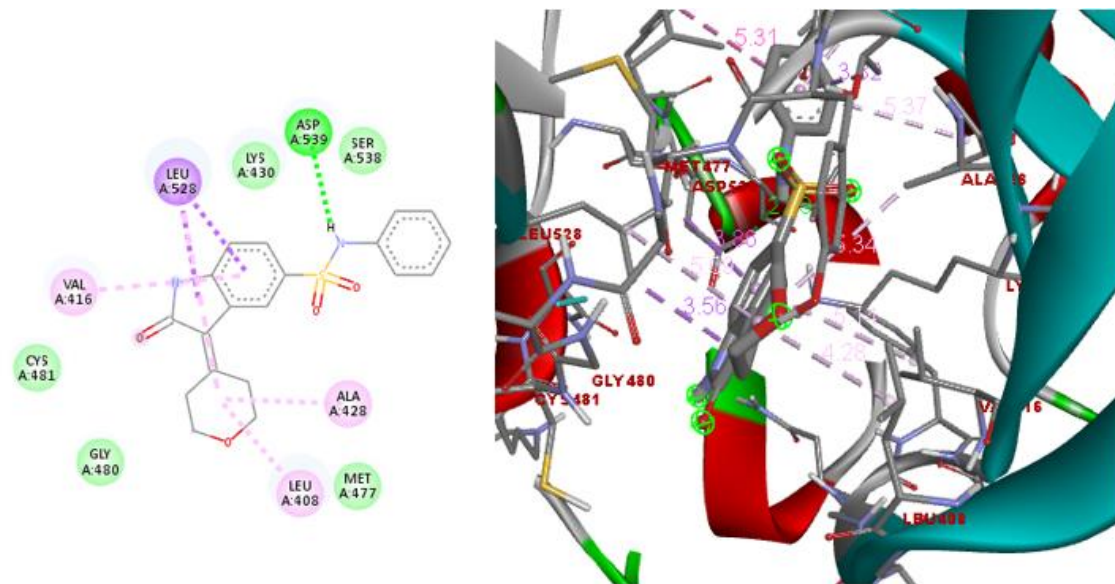


Figure 4. Molecular docking interaction of **PID-19** with BTK complexed with ibrutinib (PDB ID- 5P9J).

***In vitro* cytotoxic activity**

We chose a panel of human cell lines comprising ITK/BTK-null, ITK-positive and BTK-positive malignant cells and ITK/BTK-null non-malignant fibroblasts to test the selective cytotoxicity of derivatives. RAMOS and K562 cell lines were positive for BTK and showed no ITK expression; however, BTK expression was relatively higher in RAMOS than in K562 cells (Figure 5A). As for ITK, its expression was higher in JURKAT than in CCRF-CEM cells, and both the cell lines were negative for BTK (Figure 5A). Due to high BTK expression levels, RAMOS cells are well-recognized as a highly positive cell line for BTK.^{26,27} Other cell lines from the panel, A549, HCT116, U2OS, MRC-5 and BJ cells, did not express BTK or ITK (Figure 5A).

We next screened all 19 derivatives and ibrutinib, as a positive control, in the cell line panel following a standard procedure at our high throughput screening facility. As expected, ibrutinib showed high cytotoxicity against JURKAT, CEM-CCRF and RAMOS cells (Table 2). In addition, it was also toxic to other cancer and non-cancer cell lines. In contrast, our derivatives were inactive in ITK/BTK-null and ITK-positive cell lines, except for **PID-4**, which had a weak cytotoxic activity in CCRF-CEM cells (IC_{50} $40.87 \pm 7.95 \mu\text{M}$) (Table 2). Out of the 19 tested compounds, three showed high (**PID-4**, IC_{50} $2.29 \pm 0.52 \mu\text{M}$; **PID-6**, IC_{50} $= 9.37 \pm 2.47 \mu\text{M}$; **PID-19**, IC_{50} $= 2.64 \pm 0.88 \mu\text{M}$) to moderate (**PID-13**, IC_{50} $34.45 \pm 0.37 \mu\text{M}$ and **PID-16**, IC_{50} $30.83 \pm 3.96 \mu\text{M}$) activity in BTK-high RAMOS cells. Interestingly, these compounds showed no cytotoxicity in K562 cells, expressing low levels of BTK (Figure 5A), most probably because the bcr-abl fusion gene is a known primary driver in K562 cells.²⁸ Unlike ibrutinib, none of the compounds active in BTK-high RAMOS cells affected the growth of non-malignant cell lines. Only **PID-18**, inactive in all cancer cell lines, had moderate toxicity against MRC-5 cells (Table 2). These data show selective cytotoxicity of PID-4, PID-6 and PID-19 against BTK-high cancer cells with no off-target effects in ITK/BTK-null and ITK-positive cell lines.

Compound effect on BTK activity in RAMOS cells

Inhibition of BTK is a pivotal strategy in the field of molecular medicine, with compounds like ibrutinib and selective kinase inhibitor CHMFL-BTK-11 demonstrating their effectiveness in blocking the activation of downstream MAPK family proteins, such as p38, ERK1/2 and JNK.^{31,33} This inhibition is particularly significant in THP-1 differentiated macrophages and

RAMOS cells, where BTK is critical in orchestrating cellular responses.^{26,29}

Building upon this knowledge, we embarked on a comprehensive analysis to gauge the impact of the three most potent cytotoxic compounds—**PID-4**, **PID-6**, and **PID-19**—on the inhibition of BTK and the ensuing downstream activation of ERK1/2, JNK, and p38 in RAMOS cells. Among these compounds, our investigation unveiled that **PID-4** wielded a profound effect, significantly curtailing BTK Tyr223 phosphorylation when administered at a concentration of 50 μ M over a 24-hour period (Figure 5B and C). The inhibition of BTK by **PID-4** reverberated further downstream, as evinced by the outcomes of western blot analysis, which showcased a substantial reduction in the phosphorylation of ERK1/2, JNK, and p38 (Figure 5D). We also tested **PID-4**, **PID-6** and **PID-19** in JURKAT cells, showing that none of these compounds affected ITK levels (Figure 5E).

To further validate PID-4's effects, we subjected RAMOS cells to an initial stimulation with lipopolysaccharide (LPS), a known inducer of BTK phosphorylation and the subsequent activation of downstream MAPK family proteins.²⁹ After this initial stimulation, we administered PID-4 to the cells for 3 hours. The outcomes were remarkable, illustrating an apparent inhibitory effect of PID-4 on BTK Tyr223 phosphorylation, particularly prominent at concentrations of 10 and 50 μ M (Figure 5F and G). This reduction in BTK phosphorylation was mirrored by a corresponding decrease in the phosphorylation of ERK1/2 and JNK, predominantly noticeable at the 50 μ M concentration. Overall, the findings show a selective effect of PID-4 on BTK and downstream signalling cascades.

Conclusion

In conclusion, we embarked on the synthesis of a novel series of compounds, specifically 3-(dihydro-2H-pyran-4(3H)-ylidene)-2-oxoindoline-5-sulfonamide analogues (designated as **PID 1-19**). This synthesis was achieved through Knoevenagel condensation, wherein dihydro-2H-pyran-4(3H)-one was combined with a range of corresponding sulfonamides (denoted as **4a-s**). Importantly, this synthesis methodology proved highly efficient, consistently yielding these compounds in good quantities. The primary objective of our investigation was to explore the potential of the newly synthesized oxindole sulfonamide derivatives as promising inhibitors of cancer cell lines characterized by overactive BTK. We placed particular emphasis on assessing

the selective cytotoxicity of these compounds. Remarkably, our findings indicated that **PID-4**, **PID-6**, and **PID-19** exhibited high selectivity against BTK-high RAMOS cells, with minimal to no cytotoxicity in ITK/BTK-null cancer cell lines, ITK-positive cancer cell lines, and non-malignant cells. This crucial aspect underscores the specificity of these compounds towards BTK-high cancer cells while sparing non-malignant cells, which is a pivotal feature for potential therapeutic applications. Among the three compounds, **PID-4** stands out as a potent inhibitor of BTK-high cancer cells, demonstrating a proclivity for inhibiting the activity of BTK and subsequent downstream signalling cascade. This selective action on BTK and its associated pathways positions **PID-4** as a promising lead for further exploration and development as a potential drug for malignancies characterized by high BTK expression. This research contributes significantly to the ongoing efforts in the research and development of BTKIs, where efficacy and safety are paramount.

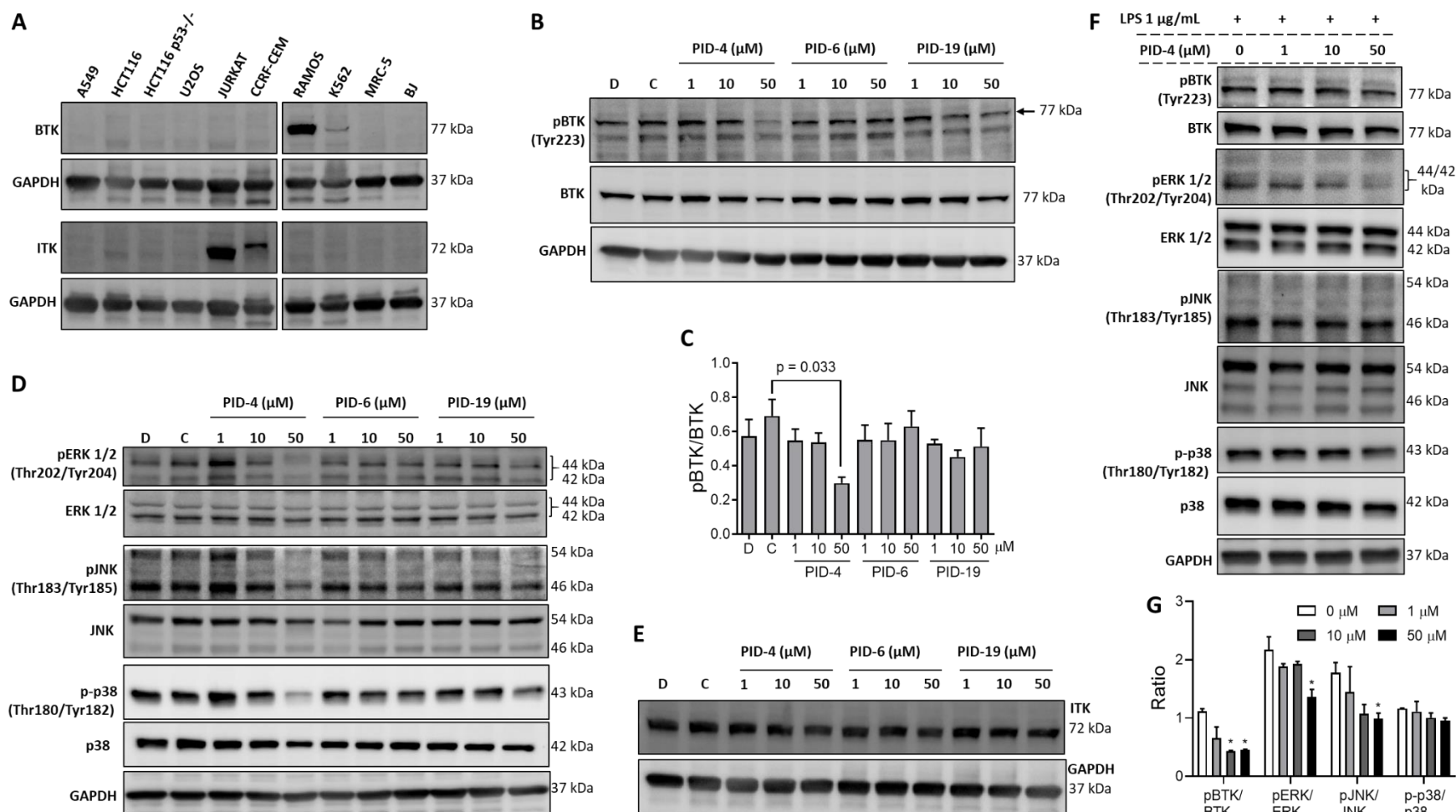


Figure 5. Compound effect on BTK and downstream signalling cascades. (A) Expression levels of BTK and ITK in cell line panel. GAPDH was used as a loading control. (B) RAMOS cells were treated with PID-4, PID-6 and PID-19 for 24 hours, and whole protein extracts were probed by Western blot for phosphorylated and total BTK. GAPDH was used as a loading control. D, DMSO treated (cells were treated with the same concentration of DMSO (0.5%) present in the highest tested drug concentration ~ 50 μM). C, Control untreated cells. (C) Graph showing the ratio of pBTK/BTK band intensities. Mean ± SEM, n = 2-4, One-way ANOVA, p = 0.033. (D) Western blot analysis of downstream signaling cascades in RAMOS cells treated with PID-4, PID-6, or PID-19 (1, 10, 50 μM) for 24 hours. Blots show pERK 1/2 (Thr202/Tyr204) (44/42 kDa), ERK 1/2 (44/42 kDa), pJNK (Thr183/Tyr185) (54/46 kDa), JNK (54/46 kDa), p-p38 (Thr180/Tyr182) (43 kDa), p38 (42 kDa), and GAPDH (37 kDa). (E) Western blot analysis of ITK phosphorylation in RAMOS cells treated with PID-4, PID-6, or PID-19 (1, 10, 50 μM) for 24 hours. Blots show ITK (72 kDa) and GAPDH (37 kDa). (F) Western blot analysis of downstream signaling cascades in RAMOS cells treated with LPS (1 μg/mL) and PID-4 (0, 1, 10, 50 μM) for 24 hours. Blots show pBTK (Tyr223) (77 kDa), BTK (77 kDa), pERK 1/2 (Thr202/Tyr204) (44/42 kDa), ERK 1/2 (44/42 kDa), pJNK (Thr183/Tyr185) (54/46 kDa), JNK (54/46 kDa), p-p38 (Thr180/Tyr182) (43 kDa), p38 (42 kDa), and GAPDH (37 kDa). (G) Bar graph showing the ratio of phosphorylated protein to total protein for pBTK/BTK, pERK/ERK, pJNK/JNK, and p-p38/p38 in RAMOS cells treated with LPS and PID-4 (0, 1, 10, 50 μM). Ratios generally decrease with increasing PID-4 concentration.

Dunnett's multiple comparison test. (D) Effect of BTK inhibition on the activation of downstream signalling pathways. (E) JURKAT cells were treated with compounds for 24 hours, and whole protein extracts were probed for ITK expression changes. (F) RAMOS cells were stimulated with LPS for 10 minutes and then treated with PID-4 for 3 hours, and changes in BTK, ERK1/2, JNK and p38 phosphorylation were probed by Western blotting of whole protein extract. (F) The ratios of pBTK/BTK, pERK1/2/ERK1/2, pJNK/JNK and p-p38/p38 band intensities are shown. Mean \pm SEM, n = 2, *p < 0.05, One-way ANOVA, Dunnett's multiple comparison test.

Table 2. Cytotoxic activity of oxindole sulfonamide derivatives. IC₅₀ values (μ M) are shown as mean \pm SD, n \geq 6.

	ITK/BTK-Null cell lines				ITK-Positive cell lines		BTK-Positive cell lines		Non-cancer	
	A549	HCT116	HCT116 p53 ^{-/-}	U2OS	Jurkat	CCRF-CEM	RAMOS	K562	MRC-5	BJ
PID-1	>50	>50	>50	>50	>50	>50	>50	>50	>50	>50
PID-2	>50	>50	>50	>50	>50	>50	>50	>50	>50	>50
PID-4	>50	>50	>50	>50	50 \pm 0	40.87 \pm 7.95	2.29 \pm 0.52	>50	>50	>50
PID-5	>50	>50	>50	>50	>50	>50	>50	>50	>50	>50
PID-6	>50	>50	>50	>50	>50	>50	9.37 \pm 2.47	>50	>50	>50
PID-7	>50	>50	>50	>50	>50	>50	>50	>50	>50	>50
PID-8	>50	>50	>50	>50	>50	>50	>50	>50	>50	>50
PID-10	>50	>50	>50	>50	>50	>50	>50	>50	>50	>50
PID-11	>50	>50	>50	>50	>50	>50	>50	>50	>50	>50
PID-12	>50	>50	>50	>50	>50	>50	>50	>50	>50	>50
PID-13	>50	>50	>50	>50	>50	>50	34.45 \pm 0.37	>50	>50	>50
PID-15	>50	>50	>50	>50	>50	>50	>50	>50	>50	>50
PID-16	>50	>50	>50	>50	>50	>50	30.83 \pm 3.96	>50	>50	>50
PID-18	>50	>50	>50	>50	>50	>50	>50	>50	33.93 \pm 6.20	>50
PID-19	>50	>50	>50	>50	>50	>50	2.64 \pm 0.88	>50	>50	>50
Ibrutinib	29.35 \pm 3.40	29.88 \pm 0.68	29.84 \pm 0.88	22.61 \pm 3.06	5.15 \pm 0.70	4.25 \pm 0.93	0.29 \pm 0.04	27.36 \pm 3.24	27.86 \pm 0.48	28.48 \pm 1.23

EXPERIMENTAL PROCEDURES

Chemistry

Materials and Methods

All reagents and solvents used to synthesize derivatives were purchased from commercial sources (Sigma Aldrich, TCI, combi-blocks). All reactions were monitored by TLC using Merck classic aluminium silica plates with size 20 x 20 cm, thickness 200 μm were detected in UV 254 nm, ninhydrine and poly molbdic acid (PMA) solutions. All compounds were purified in combi-flash chromatography using RediSep RF 1.5 Flash silica gel columns manufactured by Teledyne ISCO. Proton ^1H and ^{13}C NMR spectra were recorded on a Bruker Avance 300MHz and Ascend 400 MHz spectrometer. Proton NMR chemical shifts are reported in parts per million (δ) using TMS as a standard reference. HRMS ESI mode positive ion trap detector. IR spectra were recorded on an FT-IR spectrometer (Shimadzu FT-IR 8300 spectrophotometer), and only major peaks were reported in cm^{-1} . ^1H NMR, ^{13}C NMR, and FT-IR spectra of all compounds are provided as Supporting Information.

Procedure for synthesis of 2-oxoindoline-5-sulfonyl chloride (2): Indolin-2-one (**2**) (3.00 g, 22.5 mmol) was charged with chlorosulfonic acid (3.0 mL, 45 mmol) at 0 °C dropwise over 10 minutes. After completion addition, the reaction mixture was warmed to room temperature and stirred at 70 °C for 1 h. The reaction mixture was cooled to room temperature and poured into crushed ice (30 g), at which point, solids were precipitated. The obtained solids were filtered and dried under vacuum to obtain 2-oxoindoline-5-sulfonyl chloride (**2**) (3.75 g, 72% yield) as a light brown solid: ^1H NMR (300 MHz, $\text{DMSO}-d_6$): δ 10.55 (s, 1H), 7.49-7.46 (m, 2H), 6.79 (d, J = 7.8 Hz, 1H), 3.49 (s, 2H); LCMS (ESI+APCI): m/z = 231.9 $[\text{M} + \text{H}]^+$.

General procedure for synthesis of compound 4a-s: A solution of **2** (1.0 equiv.) in anhydrous 1, 4-dioxane was added **3a-s** (1.2 equiv.) and pyridine (3.0 equiv.) under Ar atmosphere at room temperature. After complete addition, the reaction mixture was stirred at room temperature for 2 h. The reaction mixture was diluted with water (20 mL), acidified with 2N HCl solution to pH 6 and extracted with EtOAc (3 \times 30 mL). The combined organic layer was dried over anhydrous Na_2SO_4 , filtered and concentrated under reduced pressure to obtain the crude product. The

product was washed with MTBE (20 mL) and dried under a vacuum to obtain compounds **4a-s**. These compounds were directly taken to the next step without purification.

General procedure for synthesis of compounds PID 1-19: The solution of **4a-s** (1.0 equivalent in EtOH (5.0 mL) was added **5** (1.2 equiv.) and pyrrolidine (3.0 equiv.) under Ar atmosphere at room temperature. After complete addition, the resultant reaction mixture was stirred at room temperature for 3 h. The reaction mixture was diluted with water, acidified with 2N HCl to pH 4 and extracted with EtOAc (3 x 50 mL). The combined organic layer was washed with brine solution (20 mL), dried over anhydrous Na₂SO₄, filtered and concentrated under reduced pressure to obtain the crude product. The product was purified by flash column chromatography eluted with 1-10% CH₃OH in dichloromethane to obtain **PID 1-19** derivatives with 65% to 78% yields.

3-(dihydro-2H-pyran-4(3H)-ylidene)-2-oxo-N-(tetrahydro-2H-pyran-4-yl)indoline-5-sulfonamide (PID-1): Yield: 68%; IR (KBr): ν (cm⁻¹) 3389, 3140, 2952, 1704, 1614, 1472, 1324, 1142, 1085, 921; ¹H NMR (400 MHz, DMSO-d₆): δ 10.96 (bs, 1H), 8.00 (d, *J* = 1.2 Hz, 1H), 7.70–7.66 (m, 2H), 6.97 (d, *J* = 8.4 Hz, 1H), 3.87 (t, *J* = 5.6 Hz, 2H), 3.77 (t, *J* = 5.6 Hz, 2H), 3.72–3.68 (m, 2H), 3.42 (t, *J* = 5.2 Hz, 2H), 3.24–3.10 (m, 3H), 2.96 (t, *J* = 5.2 Hz, 2H), 1.52–1.50 (m, 2H), 1.38–1.34 (m, 2H). ¹³C NMR (100 MHz, DMSO-d₆): δ 168.7, 158.6, 143.6, 134.3, 127.0, 123.2, 121.3, 119.9, 109.1, 67.4, 66.8, 65.4, 49.1, 33.2, 32.6, 29.7. HRMS (ESI): *m/z* calcd for C₁₈H₂₂N₂O₅S: 378.1249; found: 379.1312 [M + H]⁺.

N-butyl-3-(dihydro-2H-pyran-4(3H)-ylidene)-2-oxoindoline-5-sulfonamide (PID-2):

Yield: 78%; IR (KBr): ν (cm⁻¹) 3288, 2961, 2871, 1704, 1615, 1324, 1291, 1150, 920, 679; ¹H NMR (400 MHz, DMSO-d₆): δ 10.96 (bs, 1H), 7.96 (s, 1H), 7.64 (dd, *J* = 1.6, 8.2 Hz, 1H), 7.44 (t, *J* = 5.6 Hz, 1H), 6.98 (d, *J* = 8.0 Hz, 1H), 3.87 (t, *J* = 5.2 Hz, 2H), 3.77 (t, *J* = 5.6 Hz, 2H), 3.43 (t, *J* = 5.6 Hz, 2H), 2.96 (t, *J* = 5.6 Hz, 2H), 2.52 (q, *J* = 6.4 Hz, 2H), 1.35–1.30 (m, 2H), 1.28–1.20 (m, 2H), 0.79 (t, *J* = 5.6 Hz, 3H). ¹³C NMR (100 MHz, DMSO-d₆): δ 168.7, 158.6, 143.6, 132.7, 127.3, 123.2, 121.4, 119.9, 109.0, 67.4, 66.9, 42.14, 32.6, 30.9, 29.7, 13.4. HRMS (ESI): *m/z* calcd for C₁₇H₂₂N₂O₄S: 350.1300; found: 351.1373 [M + H]⁺.

***N*-cyclobutyl-3-(dihydro-2*H*-pyran-4(3*H*)-ylidene)-2-oxoindoline-5-sulfonamide (PID-3):**

Yield: 72%; IR (KBr): ν (cm⁻¹) 3288, 3158, 2866, 1688, 1614, 1324, 1144, 996, 734; ¹H NMR (300 MHz, DMSO-d₆): δ 10.96 (s, 1H), 7.95 (s, 1H), 7.84 (d, J = 8.7 Hz, 1H), 7.62 (d, J = 7.8 Hz, 1H), 6.96 (d, J = 8.7 Hz, 1H), 3.88 (t, J = 5.1 Hz, 2H), 3.77 (t, J = 5.1 Hz, 2H), 3.61–3.53 (m, 1H), 3.42 (t, J = 5.1 Hz, 2H), 2.97 (t, J = 5.1 Hz, 2H), 1.86–1.74 (m, 2H), 1.74–1.68 (m, 2H), 1.46–1.45 (m, 2H). ¹³C NMR (100 MHz, DMSO-d₆): δ 168.7, 158.5, 143.6, 133.8, 127.2, 123.1, 121.5, 119.9, 109.1, 67.4, 66.8, 47.5, 32.6, 30.5, 29.7, 14.5. HRMS (ESI): m/z calcd for C₁₇H₂₀N₂O₄S: 348.1144; found: 349.1229 [M + H]⁺.

3-(dihydro-2*H*-pyran-4(3*H*)-ylidene)-2-oxo-*N*-(*p*-tolyl)indoline-5-sulfonamide (PID-4):

Yield: 65%; IR (KBr): ν (cm⁻¹) 3369, 3205, 2874, 1708, 1615, 1472, 1327, 1142, 1079, 913; ¹H NMR (400 MHz, DMSO-d₆): δ 10.93 (bs, 1H), 10.02(bs, 1H), 7.84 (s, 1H), 7.60 (d, J = 8.0 Hz, 1H), 7.10 (t, J = 7.6 Hz, 1H), 6.94–6.83 (m, 4H), 3.82 (t, J = 5.6 Hz, 2H), 3.75 (t, J = 5.2 Hz, 2H), 3.39 (t, J = 5.6 Hz, 2H), 2.81 (t, J = 5.2 Hz, 2H), 2.20 (s, 3H). ¹³C NMR (100 MHz, DMSO-d₆): δ 168.6, 158.7, 143.9, 138.4, 137.9, 131.7, 128.9, 127.3, 124.7, 122.9, 121.5, 120.6, 119.7, 117.2, 109.1, 67.4, 66.7, 32.5, 29.6, 20.9. HRMS (ESI): m/z calcd for C₂₀H₂₀N₂O₄S: 384.1144; found: 385.1214 [M + H]⁺. HPLC purity: 99.8%, uv detection 269 nm.

3-(dihydro-2*H*-pyran-4(3*H*)-ylidene)-*N,N*-diethyl-2-oxoindoline-5-sulfonamide (PID-5):

Yield: 55%; IR (KBr): ν (cm⁻¹) 3432, 3150, 2973, 1695, 1614, 1470, 1331, 1157, 1017, 933; ¹H NMR (300 MHz, DMSO-d₆): δ 10.99 (s, 1H), 7.85 (s, 1H), 7.65 (dd, J = 1.5, 8.1 Hz, 1H), 7.00 (d, J = 8.1 Hz, 1H), 3.86 (t, J = 5.4 Hz, 2H), 3.76 (t, J = 5.4 Hz, 2H), 3.42 (t, J = 5.4 Hz, 2H), 3.18–3.11 (m, 4H), 2.93 (t, J = 5.7 Hz, 2H), 1.04 (t, J = 7.2 Hz, 6H). ¹³C NMR (100 MHz, DMSO-d₆): δ 168.6, 158.9, 143.9, 132.0, 127.5, 123.1, 121.5, 119.9, 109.5, 67.2, 66.7, 41.7, 32.6, 29.6, 14.1. HRMS (ESI): m/z calcd for C₁₇H₂₂N₂O₄S: 350.1300; found: 351.1378 [M + H]⁺.

***N*-(5-chloro-2-fluorophenyl)-3-(dihydro-2*H*-pyran-4(3*H*)-ylidene)-2-oxoindoline-5-**

sulfonamide (PID-6): Yield: 60%; IR (KBr): ν (cm⁻¹) 3243, 2859, 1703, 1616, 1490, 1339, 1173, 933, 817, 650, 523; ¹H NMR (400 MHz, DMSO-d₆): δ 11.03 (s, 1H), 10.34 (s, 1H), 7.88 (s, 1H), 7.59 (dd, J = 1.5, 8.2 Hz, 1H), 7.35–7.32 (m, 1H), 7.26–7.23 (m, 2H), 6.95 (d, J = 8.1 Hz, 1H), 3.84 (t, J = 5.4 Hz, 2H), 3.76 (t, J = 5.4 Hz, 2H), 3.40 (t, J = 5.4 Hz, 2H), 2.84 (t, J = 5.4 Hz, 2H). ¹³C NMR (100 MHz, DMSO-d₆): 168.5, 159.02, 155.0, 152.5, 144.3, 131.4, 128.1,

128.0, 127.3, 127.31, 126.3, 124.8, 123.1, 121.5, 119.7, 117.7, 109.2, 67.4, 66.7, 32.5, 29.7 δ . HRMS (ESI): m/z calcd for $C_{19}H_{16}ClFN_2O_4S$: 422.0503; found: 423.0580 $[M + H]^+$. HPLC purity: 98.1%, uv detection 269 nm.

3-(dihydro-2H-pyran-4(3H)-ylidene)-5-(pyrrolidin-1-ylsulfonyl)indolin-2-one (PID-7):

Yield: 55%; IR (KBr): ν (cm^{-1}) 3435, 2864, 1698, 1614, 1473, 1330, 1217, 1148, 1010, 712, 628; 1H NMR (400 MHz, DMSO- d_6): δ 11.02 (s, 1H), 7.86 (s, 1H), 7.67 (dd, $J = 1.6, 8.0$ Hz, 1H), 7.03 (dd, $J = 8.0$ Hz, 1H), 3.87 (t, $J = 5.6$ Hz, 2H), 3.77 (t, $J = 5.6$ Hz, 2H), 3.43 (t, $J = 5.6$ Hz, 2H), 3.12 (t, $J = 6.4$ Hz, 4H), 2.94 (t, $J = 5.6$ Hz, 2H), 1.67–1.64 (m, 4H). ^{13}C NMR (100 MHz, DMSO- d_6): δ 168.6, 159.06, 144.2, 128.2, 128.0, 123.1, 122.1, 119.9, 109.5, 67.2, 66.7, 47.7, 32.6, 29.6, 24.6. HRMS (ESI): m/z calcd for $C_{17}H_{20}N_2O_4S$: 348.1144; found: 349.1221 $[M + H]^+$.

3-(dihydro-2H-pyran-4(3H)-ylidene)-2-oxo-N-(pentan-3-yl)indoline-5-sulfonamide (PID-8):

Yield: 65%; IR (KBr): ν (cm^{-1}) 3196, 2966, 2872, 1691, 1612, 1471, 1329, 1216, 1151, 1006, 923; 1H NMR (400 MHz, DMSO- d_6): δ 10.96 (bs, 1H), 7.98 (s, 1H), 7.64 (d, $J = 8.0$ Hz, 1H), 7.37 (d, $J = 7.6$ Hz, 1H), 6.95 (d, $J = 8.0$ Hz, 1H), 3.86 (t, $J = 5.2$ Hz, 2H), 3.77 (t, $J = 5.2$ Hz, 2H), 3.42 (t, $J = 5.2$ Hz, 2H), 2.96 (t, $J = 5.2$ Hz, 2H), 2.91–2.88 (m, 1H), 1.36–1.21 (m, 4H), 0.79–0.65 (m, 6H). ^{13}C NMR (100 MHz, DMSO- d_6): δ 168.6, 158.6, 143.6, 133.8, 127.1, 123.0, 121.4, 119.9, 109.0, 67.4, 66.9, 47.5, 32.6, 30.5 (2C), 29.8, 14.9 (2C). HRMS (ESI): m/z calcd for $C_{18}H_{24}N_2O_4S$: 364.1457; found: 365.1535 $[M + H]^+$.

3-(dihydro-2H-pyran-4(3H)-ylidene)-N-(3-fluorobenzyl)-2-oxoindoline-5-sulfonamide (PID-9):

Yield: 78%; IR (KBr): ν (cm^{-1}) 3256, 3182, 2849, 1689, 1654, 1611, 1472, 1329, 1149, 1061, 923; 1H NMR (300 MHz, DMSO- d_6): δ 10.95(s, 1H), 8.13 (t, $J = 6.3$ Hz, 1H), 7.88 (s, 1H), 7.63 (dd, $J = 1.2, 8.1$ Hz, 1H), 7.32–7.24 (m, 2H), 7.07–6.98 (m, 3H), 6.94 (d, $J = 8.1$ Hz, 1H), 3.99 (d, $J = 6.3$ Hz, 2H), 3.86 (t, $J = 5.4$ Hz, 2H), 3.77 (t, $J = 5.4$ Hz, 2H), 3.42 (t, $J = 5.1$ Hz, 2H), 2.92 (t, $J = 5.4$ Hz, 2H). ^{13}C NMR (100 MHz, DMSO- d_6): 168.7, 163.2, 160.7, 158.5, 143.6, 140.6, 132.8, 130.0, 127.3, 123.5, 123.1, 121.6, 119.9, 114.2, 113.6, 109.0, 67.4, 66.8, 45.5, 32.5, 29.6. HRMS (ESI): m/z calcd for $C_{20}H_{19}FN_2O_4S$: 402.1050; found: 403.1142 $[M + H]^+$.

N-cyclohexyl-3-(dihydro-2H-pyran-4(3H)-ylidene)-2-oxoindoline-5-sulfonamide (PID-10):

Yield: 68%; IR (KBr): ν (cm^{-1}) 3324, 3210, 2936, 2862, 1706, 1617, 1469, 1321, 1145, 916,

763; ¹H NMR (300 MHz, DMSO-*d*₆): δ 10.95 (bs, 1H), 7.99 (s, 1H), 7.65 (d, *J* = 8.1 Hz, 1H), 7.52 (d, *J* = 6.9 Hz, 1H), 6.96 (d, *J* = 8.1 Hz, 1H), 3.86–3.75 (m, 4H), 3.42 (t, *J* = 5.4 Hz, 2H), 2.97–2.87 (m, 3H), 1.55–1.44 (m, 5H), 1.10–1.07 (m, 5H). ¹³C NMR (100 MHz, DMSO-*d*₆): δ 168.6, 158.6, 143.6, 132.7, 127.2, 123.1, 121.4, 119.9, 109.0, 67.4, 66.8, 42.1, 32.6, 30.9 (2C), 29.6, 23.7, 21.9 (2C). HRMS (ESI): *m/z* calcd for C₁₉H₂₄N₂O₄S: 376.1457; found: 377.1524 [M + H]⁺.

3-(dihydro-2H-pyran-4(3H)-ylidene)-N-methyl-2-oxoindoline-5-sulfonamide (PID-11):

Yield: 65%; IR (KBr): ν (cm⁻¹) 3284, 3182, 2846, 1696, 1609, 1476, 1328, 1173, 1156, 985, 923; ¹H NMR (400 MHz, DMSO-*d*₆): δ 10.94 (bs, 1H), 7.64 (d, *J* = 1.6 Hz, 1H), 7.63 (dd, *J* = 1.6, 8.4 Hz, 1H), 7.32–7.31 (m, 1H), 6.99 (d, *J* = 8.4 Hz, 1H), 3.87 (t, *J* = 5.6 Hz, 2H), 3.77 (t, *J* = 5.6 Hz, 2H), 3.43 (t, *J* = 5.6 Hz, 2H), 2.96 (t, *J* = 5.6 Hz, 2H), 2.38 (d, *J* = 4.4 Hz, 3H). ¹³C NMR (100 MHz, DMSO-*d*₆): δ 168.7, 158.6, 143.7, 131.3, 127.5, 123.2, 121.6, 119.9, 109.1, 67.4, 66.8, 32.6, 29.7, 28.6. HRMS (ESI): *m/z* calcd for C₁₄H₁₆N₂O₄S: 308.0831; found: 309.0904 [M + H]⁺.

3-(dihydro-2H-pyran-4(3H)-ylidene)-2-oxo-N-(tetrahydrofuran-3-yl)indoline-5-

sulfonamide (PID-12): Yield: 65%; IR (KBr): ν (cm⁻¹) 3436, 2865, 1693, 1614, 1474, 1324, 1152, 1080, 923, 736, 615; ¹H NMR (300 MHz, DMSO-*d*₆): δ 10.99 (bs, 1H), 7.99 (s, 1H), 7.81 (d, *J* = 5.4 Hz, 1H), 7.67 (d, *J* = 8.1 Hz, 1H), 6.99 (d, *J* = 7.8 Hz, 1H), 3.88–3.78 (m, 4H), 3.70–3.56 (m, 5H), 3.41–3.42 (m, 2H), 2.98–2.92 (m, 2H), 1.90–1.84 (m, 1H), 1.78–1.66 (m, 1H). ¹³C NMR (100 MHz, DMSO-*d*₆): δ 168.7, 158.8, 143.8, 133.1, 127.4, 123.2, 121.5, 119.9, 109.2, 71.9, 67.4, 66.8, 66.1, 53.0, 32.6, 32.0, 29.7. HRMS (ESI): *m/z* calcd for C₁₇H₂₀N₂O₅S: 364.1093; found: 365.1171 [M + H]⁺.

3-(dihydro-2H-pyran-4(3H)-ylidene)-5-(morpholinosophonyl)indolin-2-one (PID-13):

Yield: 68%; IR (KBr): ν (cm⁻¹); ¹H NMR (400 MHz, DMSO-*d*₆): δ 11.06 (s, 1H), 7.79 (d, *J* = 1.6 Hz, 1H), 7.59 (dd, *J* = 1.6, 8.2 Hz, 1H), 7.06 (d, *J* = 8.2 Hz, 1H), 3.86 (t, *J* = 5.6 Hz, 2H), 3.77 (t, *J* = 5.6 Hz, 2H), 3.63 (t, *J* = 4.8 Hz, 4H), 3.43 (t, *J* = 5.6 Hz, 2H), 2.94 (t, *J* = 5.6 Hz, 2H), 2.86 (t, *J* = 4.4 Hz, 4H). ¹³C NMR (100 MHz, DMSO-*d*₆): δ 168.7, 159.4, 144.5, 128.4, 126.4, 123.3, 122.4, 119.8, 109.5, 67.2, 66.7, 65.3, 45.8, 32.6, 29.6. HRMS (ESI): *m/z* calcd for C₁₇H₂₀N₂O₅S: 364.1093; found: 365.1171 [M + H]⁺.

***N*-benzyl-3-(dihydro-2*H*-pyran-4(3*H*)-ylidene)-2-oxoindoline-5-sulfonamide (PID-14):**

Yield: 70%; IR (KBr): ν (cm⁻¹) 3162, 2853, 1698, 1607, 1473, 1350, 1222, 1173, 1109, 940, 741, 633; ¹H NMR (300 MHz, DMSO-*d*₆): δ 10.95 (s, 1H), 8.03 (t, *J* = 6.3 Hz, 1H), 7.91 (s, 1H), 7.65 (dd, *J* = 1.2, 8.1 Hz, 1H), 7.28–7.18 (m, 5H), 6.95 (d, *J* = 8.1 Hz, 1H), 3.94 (d, *J* = 6.3 Hz, 2H), 3.86 (t, *J* = 5.4 Hz, 2H), 3.77 (t, *J* = 5.4 Hz, 2H), 3.42 (t, *J* = 5.4 Hz, 2H), 2.92 (t, *J* = 5.4 Hz, 2H). ¹³C NMR (100 MHz, DMSO-*d*₆): δ 168.7, 158.5, 143.6, 137.5, 132.8, 128.1, 127.6, 127.3, 127.0, 123.1, 121.6, 119.9, 109.0, 67.4, 66.9, 46.1, 32.6, 29.6. HRMS (ESI): *m/z* calcd for C₂₀H₂₀N₂O₄S: 384.1144; found: 385.1214 [M + H]⁺.

4-(3-(dihydro-2*H*-pyran-4(3*H*)-ylidene)-2-oxoindoline-5-sulfonamido)benzoic acid (PID-15):

Yield: 75%; IR (KBr): ν (cm⁻¹) 3270, 2862, 1691, 1607, 1471, 1336, 1223, 1150, 921, 771; ¹H NMR (300 MHz, DMSO-*d*₆): δ 12.75 (bs, 1H), 11.0 (s, 1H), 10.64 (s, 1H), 7.90 (s, 1H), 7.81 (d, *J* = 8.4 Hz, 2H), 7.67 (dd, *J* = 1.2, 8.0 Hz, 1H), 7.22 (d, *J* = 8.4 Hz, 2H), 6.94 (d, *J* = 8.0 Hz, 1H), 3.81 (t, *J* = 5.6 Hz, 2H), 3.74 (t, *J* = 5.6 Hz, 2H), 3.38 (t, *J* = 5.6 Hz, 2H), 2.83 (t, *J* = 5.6 Hz, 2H). ¹³C NMR (100 MHz, DMSO-*d*₆): δ 168.6, 116.7, 159.2, 144.3, 144.2, 131.3, 130.8 (2C), 127.5, 125.7, 123.2, 121.4, 119.7, 118.5 (2C), 109.3, 67.4, 66.8, 32.6, 29.7. HRMS (ESI): *m/z* calcd for C₂₀H₁₈N₂O₆S: 414.0886; found: 415.7762 [M + H]⁺.

***N*-(cyclopropylmethyl)-3-(dihydro-2*H*-pyran-4(3*H*)-ylidene)-2-oxoindoline-5-sulfonamide (PID-16):**

Yield: 69%; IR (KBr): ν (cm⁻¹) 3233, 3168, 2871, 1697, 1608, 1471, 1323, 1149, 1065, 826, 796; ¹H NMR (300 MHz, DMSO-*d*₆): δ 10.88 (bs, 1H), 7.91 (s, 1H), 7.58–7.53 (m, 2H), 6.89 (d, *J* = 8.1 Hz, 1H), 3.80 (t, *J* = 4.8 Hz, 2H), 3.70 (t, *J* = 5.1 Hz, 2H), 3.35 (t, *J* = 5.1 Hz, 2H), 2.89 (t, *J* = 4.8 Hz, 2H), 2.53 (t, *J* = 6.3 Hz, 2H), 0.70–0.66 (m, 1H), 0.28–0.26 (m, 2H)–0.00–0.06 (m, 2H). ¹³C NMR (100 MHz, DMSO-*d*₆): δ 168.7, 158.6, 143.5, 133.1, 127.2, 123.1, 121.5, 119.9, 67.4, 66.9, 47.2, 32.6, 29.6, 10.5, 3.4. HRMS (ESI): *m/z* calcd for C₁₇H₂₀N₂O₄S: 348.1144; found: 349.1219 [M + H]⁺. HPLC purity: 99.2%, uv detection 266 nm.

3-(dihydro-2*H*-pyran-4(3*H*)-ylidene)-*N*-(2-methoxyethyl)-2-oxoindoline-5-sulfonamide (PID-17):

Yield: 55%; IR (KBr): ν (cm⁻¹) 3374, 2858, 1694, 1613, 1473, 1324, 1217, 1153, 1082, 961, 713; ¹H NMR (300 MHz, DMSO-*d*₆): δ 10.96 (bs, 1H), 7.98 (s, 1H), 7.65–7.58 (m, 2H), 6.97 (d, *J* = 8.1 Hz, 1H), 3.87–3.85 (m, 2H), 3.77–3.75 (m, 2H), 3.44–3.42 (m, 2H), 3.29 (t, *J* = 5.7 Hz, 2H), 3.16 (s, 3H), 2.98–2.96 (m, 2H), 2.85 (q, *J* = 5.4 Hz, 2H). ¹³C NMR (100 MHz,

DMSO- d_6): δ 168.7, 158.6, 143.6, 132.8, 127.2, 123.2, 121.5, 119.9, 109.0, 67.4, 66.9, 57.8, 42.1, 32.6, 29.7. HRMS (ESI): m/z calcd for $C_{16}H_{20}N_2O_5S$: 352.1093; found: 353.1164 [M + H]⁺.

3-(dihydro-2H-pyran-4(3H)-ylidene)-N-(3-methoxyphenyl)-2-oxoindoline-5-sulfonamide

(PID-18): Yield: 65%; IR (KBr): ν (cm^{-1}) 3381, 3206, 2873, 1708, 1608, 1472, 1324, 1140, 1114, 912, 791; ¹H NMR (300 MHz, DMSO- d_6): δ 10.89 (bs, 1H), 10.19 (bs, 1H), 7.88 (s, 1H), 7.62 (d, J = 8.1 Hz, 1H), 7.13 (t, J = 8.1 Hz, 1H), 6.93 (d, J = 8.1 Hz, 1H), 6.70–6.67 (m, 2H), 6.60 (d, J = 7.5 Hz, 1H), 3.83 (t, J = 4.8 Hz, 2H), 3.75 (t, J = 5.4 Hz, 2H), 3.69 (s, 3H), 3.39 (t, J = 5.1 Hz, 2H), 2.83 (t, J = 4.8 Hz, 2H). ¹³C NMR (100 MHz, DMSO- d_6): δ 168.6, 163.1, 160.7, 158.5, 143.6, 140.6, 140.5, 132.8, 130.0, 129.9, 127.2, 123.5, 121.6, 114.2, 113.5, 67.4, 66.8, 45.5, 32.5, 29.6. HRMS (ESI): m/z calcd for $C_{20}H_{20}N_2O_5S$: 400.1093; found: 401.1163 [M + H]⁺.

3-(dihydro-2H-pyran-4(3H)-ylidene)-2-oxo-N-phenylindoline-5-sulfonamide (PID-19):

Yield: 75%; IR (KBr): ν (cm^{-1}) 3383, 3214, 2873, 1710, 1619, 1475, 1333, 1144, 1114, 912, 765; ¹H NMR (400 MHz, DMSO- d_6): δ 10.96 (s, 1H), 10.09 (s, 1H), 7.83 (s, 2H), 7.59 (dd, J = 1.6, 8.0 Hz, 1H), 7.23 (t, J = 7.6 Hz, 2H), 7.11–7.09 (m, 2H), 7.03 (t, J = 7.2 Hz, 1H), 6.91 (d, J = 8.0 Hz, 1H), 3.82 (t, J = 5.6 Hz, 2H), 3.74 (t, J = 5.6 Hz, 2H), 3.38 (t, J = 5.2 Hz, 2H), 2.80 (t, J = 5.2 Hz, 2H). ¹³C NMR (100 MHz, DMSO- d_6): δ 168.5, 158.8, 143.9, 137.9, 131.5, 129.1, 127.3, 123.0, 121.4, 120.4, 119.7, 109.1, 67.4, 66.8, 32.5, 29.6. HRMS (ESI): m/z calcd for $C_{19}H_{18}N_2O_4S$: 370.0987; found: 371.1046 [M + H]⁺. HPLC purity: 99.7%, uv detection 266 nm.

Computational section

Preparation of protein/receptor

The crystalline structure of BTK complexed with an inhibitor Ibrutinib (PDB ID- 5P9J)³⁴ with resolution 2.5 Å was downloaded from Research Collaboratory for Structural Bioinformatics (RCSB) which is the protein data bank database (www.rcsb.org), in .pdb format. The protein was created using the AutoDock programme.³⁰ It has a single chain, which was chosen as the target of the study. The natural ligand, non-interacting ions, and water molecules were all removed from the crystal structure. In order to reduce the strain on the crystal structure and make the protein usable in the AutoDock docking simulation tool, the lacking hydrogens were added. The protein was created using the UCSF Chimera graphical user interface after the structural

reduction, which includes hydrogen atoms, Gasteiger charge calculations, and the merging of the non-polar hydrogens to carbon atoms.

ChemSketch

ChemSketch is a programme specialized for sketching chemical structures by focusing on chemical structure data. It aids in the two-dimensional drawing of compounds, which can then be quickly transformed into three dimensions using a three-dimensional algorithm that also considers the molecular dynamics of such compounds. In the domains of bioinformatics and cheminformatics, it is extensively employed. ChemSketch has been utilized in order to create analogues of the chemicals. Using UCSF Chimera, ligand input files were created for docking and saved in mol2 file format.³¹

Chimera

The interactions were visualized and examined using UCSF Chimera, which can be extended to analyze molecular structures and associated data such as density maps, sequence alignment outcomes, docking outcomes, and trajectory findings. It offers a high degree of functionality in addition to fundamental functions, such as visualization and extension.³²

Discovery studio

The Discovery Studio assists in determining the types of interactions and bond lengths between the active sites in the target and ligand conformations. BIOVIA Discovery Studio Visualizer (Accelrys) is a unified, user-friendly graphical interface for effective drug design and protein modelling.

Docking

The molecular docking method was applied to the selected ligands with the help of AutoDock Vina.^[33] A grid box for BTK with the dimensions X:30, Y:30, Z:30 Å and a grid spacing of 1.0 Å focused on X: 18.309, Y:9.2081, Z: 7.9357 was identified as the protein target docking site, and best molecular interacting compounds were observed. The interactions between the active sites in the target and ligand conformation, along with the type of interaction and bond distances, were identified using Discovery Studio Visualizer.

Biology

Cell lines

Cells were either purchased from ATCC (Middlesex, UK) or DSMZ (Braunschweig, Germany) and maintained at 37°C in a humidified incubator (5% CO₂/atmospheric air) in recommended growth medium supplemented with 10% fetal calf serum, antibiotics (100 mg/mL streptomycin and 100 U/mL penicillin), 2 mM glutamine, 1 mM NaHCO₃, 1 mM C₃H₃NaO₃, and 20 mM HEPES. Cell lines were regularly validated and checked for mycoplasma infection every two weeks.

Cytotoxicity assay

The cytotoxicity of compounds was tested using an MTS assay protocol developed for routine compound screening at our facility, and IC₅₀ values were calculated, as described previously.³³

Drug treatment and Western blotting analysis

RAMOS and JURKAT cells were plated at 0.5 x 10⁶/mL density in 6-well cell culture plates in complete growth media and treated with PID-4, PID-6 and PID-19 at 1-50 μM concentrations for 24 hours. For LPS stimulation, RAMOS cells in a growth medium containing 1% FCS were exposed to 1 μg/ml LPS for 10 minutes. Cells were next centrifuged to remove LPS-containing media and washed twice with complete growth media containing 10% FCS. Stimulated cells were next plated at a density of 0.5 x 10⁶/mL in 6-well plates, followed by treatment with PID-4 for 3 hours.

To prepare whole protein extracts, cells following treatment were collected by centrifugation and lysed in RIPA buffer (Thermo Fisher Scientific, Massachusetts, USA) supplemented with protease (Cat. #04693116001) and phosphatase (Cat. #04906837001) inhibitors from Roche, Basel, Switzerland by sonication on a Cup Horn sonicator (Qsonica, LLC., Connecticut, USA). Sonicated samples were centrifuged at 12 000 RPM for 30 min at 4 °C, and the supernatants were collected in fresh Eppendorf tubes. Thirty-five μg of protein lysates were electrophoresed by 10% SDS-PAGE and processed for Western blotting following a standard protocol.

Membranes were probed with following primary antibodies purchased from Cell Signaling Technology, Inc. (Massachusetts, USA) for overnight at 4 °C or 1 h at room temperature: Total BTK (1:1000; Cat # 3533S), Phosphor-BTK (Tyr223) (1:1000; Cat # 5082S), p44/42 MAPK (ERK1/2) (1:1000; Cat # 9102S), Phospho-p44/42 MAPK (ERK1/2) (Thr202/Tyr204) (1:1000; Cat # 4376S), p38 MAPK (1:1000; Cat # 9212S), Phospho-p38 MAPK (Thr180/Tyr182) (1:1000; Cat # 9211S), SAPK/JNK (1:1000; Cat # 9252S), Phospho-SAPK/JNK (Thr183/Tyr185) (G9) (1:1000; Cat # 9255S), ITK (1:1000; Cat #2380S) and GAPDH (14C10) (1:4000; Cat # 2118S). Blots with primary antibodies were developed using anti-mouse, or anti-rabbit IgG secondary antibodies conjugated to Alexa Fluor 488 (1:2000; Cat #A11034 and A21202; Invitrogen, Massachusetts, USA) for 1–2 h at room temperature in the dark. Protein bands were visualized on a Gel Doc XR + Gel Documentation System (Bio-Rad, California, USA).

Statistical analysis

All blots were analyzed using NIH ImageJ software (Bethesda, Maryland, USA). All statistical analyses were performed in Statistica Version 14 (TIBCO Software Inc., CA, USA), and differences were considered significant at $P < 0.05$.

ASSOCIATED CONTENT

Supporting Information: ^1H NMR, ^{13}C NMR, HRMS, HPLC, and FT-IR spectra of all compounds (PDF).

AUTHOR INFORMATION

***Corresponding Authors**

Viswanath Das – *Institute of Molecular and Translational Medicine, Faculty of Medicine and Dentistry, Palacký University Olomouc, Hněvotínská 1333/5, 77900 Olomouc, Czech Republic;* ORCID: orcid.org/0000-0001-5973-5990; Email: viswanath.das@upol.cz

Rambabu Gundla – *Department of Chemistry, School of Science, GITAM (Deemed to be University) Hyderabad, Telangana - 502 329, India;* ORCID: orcid.org/0000-0003-0390-6505; Email: rgundla@gitam.edu

Authors

Chandra Prakash Koraboina – *Department of Chemistry, School of Science, GITAM (Deemed to be University) Hyderabad, Telangana - 502 329, India*

Venkatanarayana Chowdary Maddipati – *Department of Chemistry, School of Science, GITAM (Deemed to be University) Hyderabad, Telangana - 502 329, India*

Narendran Annadurai - *Institute of Molecular and Translational Medicine, Faculty of Medicine and Dentistry, Palacký University Olomouc, Hněvotínská 1333/5, 77900 Olomouc, Czech Republic*

Soňa Gurská - *Institute of Molecular and Translational Medicine, Faculty of Medicine and Dentistry, Palacký University Olomouc, Hněvotínská 1333/5, 77900 Olomouc, Czech Republic*

Petr Džubák - *Institute of Molecular and Translational Medicine, Faculty of Medicine and Dentistry, Palacký University Olomouc, Hněvotínská 1333/5, 77900 Olomouc, Czech Republic*

Marián Hajdúch - *Institute of Molecular and Translational Medicine, Faculty of Medicine and Dentistry, Palacký University Olomouc, Hněvotínská 1333/5, 77900 Olomouc, Czech Republic*

Author Contributions

Conceptualization, C.P.K., V.C.M. and R.G.; methodology, C.P.K., V.C.M., N.A. and S.G.; Investigation, C.P.K., V.C.M., N.A., S.G. and V.D.; Writing – original draft preparation, C.P.K., V.D. and R.G.; Writing – review and editing, M.H., V.D. and R.G.; Supervision, V.D. and R.G.; Project administration, V.D. and R.G.; Funding acquisition, P.D., M.H., V.D. and R.G.

ACKNOWLEDGMENTS

The research was funded by the Department of Science and Technology, India (DST-SERB-EDCR/2016/000288) for financial assistance. The authors thanks Gandhi Institute of Technology (GITAM) for the research facility. The biological part of the study was supported by infrastructural projects (CZ-OPENSREEN – LM2023052; EATRIS-CZ – LM2023053), the projects National Institute for Cancer Research (Project No. LX22NPO5102) and National

Institute for Neurological Research (Project No. LX22NPO5107) - Funded by the European Union - Next Generation EU from the Ministry of Education, Youth and Sports of the Czech Republic (MEYS).

NOTES

The authors declare no conflict of financial interests.

DATA AVAILABILITY STATEMENT

The raw data supporting this study's findings are available upon reasonable request from the corresponding authors.

REFERENCES

- (1) Wang, X.; Kokabee, L.; Kokabee, M.; Conklin, D. S. Bruton's Tyrosine Kinase and Its Isoforms in Cancer. *Frontiers in Cell and Developmental Biology* **2021**, *9*.
- (2) Seiler, T.; Dreyling, M. Bruton's Tyrosine Kinase Inhibitors in B-Cell Lymphoma: Current Experience and Future Perspectives. *Expert Opinion on Investigational Drugs* **2017**, *26* (8), 909–915. <https://doi.org/10.1080/13543784.2017.1349097>.
- (3) Middendorp, S.; Dingjan, G. M.; Maas, A.; Dahlenborg, K.; Hendriks, R. W. Function of Bruton's Tyrosine Kinase during B Cell Development Is Partially Independent of Its Catalytic Activity 1. *The Journal of Immunology* **2003**, *171* (11), 5988–5996. <https://doi.org/10.4049/jimmunol.171.11.5988>.
- (4) Lee, J.; Rhee, M.; Min, T. K.; Bang, H. I.; Jang, M.-A.; Kang, E.-S.; Kim, H.-J.; Yang, H.-J.; Pyun, B. Y. A Novel BTK Gene Mutation, c.82delC (p.Arg28 Alafs*5), in a Korean Family with X-Linked Agammaglobulinemia. *Korean J Pediatr* **2016**, *59* (Suppl 1), S49–S52. <https://doi.org/10.3345/kjp.2016.59.11.S49>.
- (5) Sung, H.; Ferlay, J.; Siegel, R. L.; Laversanne, M.; Soerjomataram, I.; Jemal, A.; Bray, F. Global Cancer Statistics 2020: GLOBOCAN Estimates of Incidence and Mortality Worldwide for 36 Cancers in 185 Countries. *CA: A Cancer Journal for Clinicians* **2021**, *71* (3), 209–249. <https://doi.org/10.3322/caac.21660>.
- (6) Anand, U.; Dey, A.; Chandel, A. K. S.; Sanyal, R.; Mishra, A.; Pandey, D. K.; De Falco, V.; Upadhyay, A.; Kandimalla, R.; Chaudhary, A.; Dhanjal, J. K.; Dewanjee, S.;

- Vallamkondu, J.; Pérez de la Lastra, J. M. Cancer Chemotherapy and beyond: Current Status, Drug Candidates, Associated Risks and Progress in Targeted Therapeutics. *Genes & Diseases* **2023**, *10* (4), 1367–1401. <https://doi.org/10.1016/j.gendis.2022.02.007>.
- (7) Garraway, L. A.; Jänne, P. A. Circumventing Cancer Drug Resistance in the Era of Personalized Medicine. *Cancer Discovery* **2012**, *2* (3), 214–226. <https://doi.org/10.1158/2159-8290.CD-12-0012>.
- (8) Srivastava, S.; Koay, E. J.; Borowsky, A. D.; De Marzo, A. M.; Ghosh, S.; Wagner, P. D.; Kramer, B. S. Cancer Overdiagnosis: A Biological Challenge and Clinical Dilemma. *Nature Reviews Cancer* **2019**, *19* (6), 349–358. <https://doi.org/10.1038/s41568-019-0142-8>.
- (9) Hanahan, D.; Weinberg, R. A. Hallmarks of Cancer: The next Generation. *Cell* **2011**, *144*. <https://doi.org/10.1016/j.cell.2011.02.013>.
- (10) Ammann, E. M.; Shanafelt, T. D.; Wright, K. B.; McDowell, B. D.; Link, B. K.; Chrischilles, E. A. Updating Survival Estimates in Patients with Chronic Lymphocytic Leukemia or Small Lymphocytic Lymphoma (CLL/SLL) Based on Treatment-Free Interval Length. *Leukemia & Lymphoma* **2018**, *59* (3), 643–649. <https://doi.org/10.1080/10428194.2017.1349905>.
- (11) Cheah, C. Y.; Seymour, J. F.; Wang, M. L. Mantle Cell Lymphoma. *JCO* **2016**, *34* (11), 1256–1269. <https://doi.org/10.1200/JCO.2015.63.5904>.
- (12) Chang, B. Y.; Francesco, M.; De Rooij, M. F. M.; Magadala, P.; Steggerda, S. M.; Huang, M. M.; Kuil, A.; Herman, S. E. M.; Chang, S.; Pals, S. T.; Wilson, W.; Wiestner, A.; Spaargaren, M.; Buggy, J. J.; Elias, L. Egress of CD19+CD5+ Cells into Peripheral Blood Following Treatment with the Bruton Tyrosine Kinase Inhibitor Ibrutinib in Mantle Cell Lymphoma Patients. *Blood* **2013**, *122* (14), 2412–2424. <https://doi.org/10.1182/blood-2013-02-482125>.
- (13) Treon, S. P.; Xu, L.; Yang, G.; Zhou, Y.; Liu, X.; Cao, Y.; Sheehy, P.; Manning, R. J.; Patterson, C. J.; Tripsas, C.; Arcaini, L.; Pinkus, G. S.; Rodig, S. J.; Sohani, A. R.; Harris, N. L.; Laramie, J. M.; Skifter, D. A.; Lincoln, S. E.; Hunter, Z. R. MYD88 L265P Somatic Mutation in Waldenström’s Macroglobulinemia. *N Engl J Med* **2012**, *367* (9), 826–833. <https://doi.org/10.1056/NEJMoa1200710>.
- (14) Krysiak, K.; Gomez, F.; White, B. S.; Matlock, M.; Miller, C. A.; Trani, L.; Fronick, C. C.; Fulton, R. S.; Kreisel, F.; Cashen, A. F.; Carson, K. R.; Berrien-Elliott, M. M.; Bartlett, N.

- L.; Griffith, M.; Griffith, O. L.; Fehniger, T. A. Recurrent Somatic Mutations Affecting B-Cell Receptor Signaling Pathway Genes in Follicular Lymphoma. *Blood* **2017**, *129* (4), 473–483. <https://doi.org/10.1182/blood-2016-07-729954>.
- (15) Vetrie, D.; Vořechovský, I.; Sideras, P.; Holland, J.; Davies, A.; Flinter, F.; Hammarström, L.; Kinnon, C.; Levinsky, R.; Bobrow, M.; Smith, C. I. E.; Bentley, D. R. The Gene Involved in X-Linked Agammaglobulinaemia Is a Member of the Src Family of Protein-Tyrosine Kinases. *Nature* **1993**, *361* (6409), 226–233. <https://doi.org/10.1038/361226a0>.
- (16) Tsukada, S.; Saffran, D. C.; Rawlings, D. J.; Parolini, O.; Allen, R. C.; Klisak, I.; Sparkes, R. S.; Kubagawa, H.; Mohandas, T.; Quan, S.; Belmont, J. W.; Cooper, M. D.; Conley, M. E.; Witte, O. N. Deficient Expression of a B Cell Cytoplasmic Tyrosine Kinase in Human X-Linked Agammaglobulinemia. *Cell* **1993**, *72* (2), 279–290. [https://doi.org/10.1016/0092-8674\(93\)90667-F](https://doi.org/10.1016/0092-8674(93)90667-F).
- (17) Pal Singh, S.; Dammeijer, F.; Hendriks, R. W. Role of Bruton's Tyrosine Kinase in B Cells and Malignancies. *Molecular Cancer* **2018**, *17* (1), 57. <https://doi.org/10.1186/s12943-018-0779-z>.
- (18) Tasso, B.; Spallarossa, A.; Russo, E.; Brullo, C. The Development of BTK Inhibitors: A Five-Year Update. *Molecules* **2021**, *26* (23). <https://doi.org/10.3390/molecules26237411>.
- (19) Jain, P.; Keating, M.; Wierda, W.; Estrov, Z.; Ferrajoli, A.; Jain, N.; George, B.; James, D.; Kantarjian, H.; Burger, J.; O'Brien, S. Outcomes of Patients with Chronic Lymphocytic Leukemia after Discontinuing Ibrutinib. *Blood* **2015**, *125* (13), 2062–2067. <https://doi.org/10.1182/blood-2014-09-603670>.
- (20) Molina-Cerrillo, J.; Alonso-Gordoa, T.; Gajate, P.; Grande, E. Bruton's Tyrosine Kinase (BTK) as a Promising Target in Solid Tumors. *Cancer Treatment Reviews* **2017**, *58*, 41–50. <https://doi.org/10.1016/j.ctrv.2017.06.001>.
- (21) De Cesco, S.; Kurian, J.; Dufresne, C.; Mittermaier, A. K.; Moitessier, N. Covalent Inhibitors Design and Discovery. *European Journal of Medicinal Chemistry* **2017**, *138*, 96–114. <https://doi.org/10.1016/j.ejmech.2017.06.019>.
- (22) Alu, A.; Lei, H.; Han, X.; Wei, Y.; Wei, X. BTK Inhibitors in the Treatment of Hematological Malignancies and Inflammatory Diseases: Mechanisms and Clinical Studies. *Journal of Hematology & Oncology* **2022**, *15* (1), 138. <https://doi.org/10.1186/s13045-022-01353-w>.

- (23) Bender, A. T.; Gardberg, A.; Pereira, A.; Johnson, T.; Wu, Y.; Grenningloh, R.; Head, J.; Morandi, F.; Haselmayer, P.; Liu-Bujalski, L. Ability of Bruton's Tyrosine Kinase Inhibitors to Sequester Y551 and Prevent Phosphorylation Determines Potency for Inhibition of Fc Receptor but Not B-Cell Receptor Signaling. *Mol Pharmacol* **2017**, *91* (3), 208. <https://doi.org/10.1124/mol.116.107037>.
- (24) Guo, Y.; Liu, Y.; Hu, N.; Yu, D.; Zhou, C.; Shi, G.; Zhang, B.; Wei, M.; Liu, J.; Luo, L.; Tang, Z.; Song, H.; Guo, Y.; Liu, X.; Su, D.; Zhang, S.; Song, X.; Zhou, X.; Hong, Y.; Chen, S.; Cheng, Z.; Young, S.; Wei, Q.; Wang, H.; Wang, Q.; Lv, L.; Wang, F.; Xu, H.; Sun, H.; Xing, H.; Li, N.; Zhang, W.; Wang, Z.; Liu, G.; Sun, Z.; Zhou, D.; Li, W.; Liu, L.; Wang, L.; Wang, Z. Discovery of Zanubrutinib (BGB-3111), a Novel, Potent, and Selective Covalent Inhibitor of Bruton's Tyrosine Kinase. *J. Med. Chem.* **2019**, *62* (17), 7923–7940. <https://doi.org/10.1021/acs.jmedchem.9b00687>.
- (25) Johnson, A. R.; Kohli, P. B.; Katewa, A.; Gogol, E.; Belmont, L. D.; Choy, R.; Penuel, E.; Burton, L.; Eigenbrot, C.; Yu, C.; Ortwine, D. F.; Bowman, K.; Franke, Y.; Tam, C.; Estevez, A.; Mortara, K.; Wu, J.; Li, H.; Lin, M.; Bergeron, P.; Crawford, J. J.; Young, W. B. Battling Btk Mutants With Noncovalent Inhibitors That Overcome Cys481 and Thr474 Mutations. *ACS Chem. Biol.* **2016**, *11* (10), 2897–2907. <https://doi.org/10.1021/acscchembio.6b00480>.
- (26) Chu, Y.; Lee, S.; Shah, T.; Yin, C.; Barth, M.; Miles, R. R.; Ayello, J.; Morris, E.; Harrison, L.; Van de Ven, C.; Galardy, P.; Goldman, S. C.; Lim, M. S.; Hermiston, M.; McAllister-Lucas, L. M.; Giulino-Roth, L.; Perkins, S. L.; Cairo, M. S. Ibrutinib Significantly Inhibited Bruton's Tyrosine Kinase (BTK) Phosphorylation, in-Vitro Proliferation and Enhanced Overall Survival in a Preclinical Burkitt Lymphoma (BL) Model. *OncImmunology* **2019**, *8* (1), e1512455. <https://doi.org/10.1080/2162402X.2018.1512455>.
- (27) Turetsky, A.; Kim, E.; Kohler, R. H.; Miller, M. A.; Weissleder, R. Single Cell Imaging of Bruton's Tyrosine Kinase Using an Irreversible Inhibitor. *Scientific Reports* **2014**, *4* (1), 4782. <https://doi.org/10.1038/srep04782>.
- (28) Pastwa, E.; Somiari, R. I.; Malinowski, M.; Somiari, S. B.; Winters, T. A. In Vitro Non-Homologous DNA End Joining Assays—The 20th Anniversary. *The International Journal of Biochemistry & Cell Biology* **2009**, *41* (6), 1254–1260. <https://doi.org/10.1016/j.biocel.2008.11.007>.

- (29) Ping, L.; Ding, N.; Shi, Y.; Feng, L.; Li, J.; Liu, Y.; Lin, Y.; Shi, C.; Wang, X.; Pan, Z.; Song, Y.; Zhu, J. The Bruton's Tyrosine Kinase Inhibitor Ibrutinib Exerts Immunomodulatory Effects through Regulation of Tumor-Infiltrating Macrophages. *Oncotarget*; Vol 8, No 24 **2017**.
- (30) Morris, G. M.; Huey, R.; Lindstrom, W.; Sanner, M. F.; Belew, R. K.; Goodsell, D. S.; Olson, A. J. AutoDock4 and AutoDockTools4: Automated Docking with Selective Receptor Flexibility. *Journal of Computational Chemistry* **2009**, 30 (16), 2785–2791. <https://doi.org/10.1002/jcc.21256>.
- (31) Hunter, A. D. ACD/ChemSketch 1.0 (Freeware); ACD/ChemSketch 2.0 and Its Tautomers, Dictionary, and 3D Plug-Ins; ACD/HNMR 2.0; ACD/CNMR 2.0. *J. Chem. Educ.* **1997**, 74 (8), 905. <https://doi.org/10.1021/ed074p905>.
- (32) Pettersen, E. F.; Goddard, T. D.; Huang, C. C.; Couch, G. S.; Greenblatt, D. M.; Meng, E. C.; Ferrin, T. E. UCSF Chimera—A Visualization System for Exploratory Research and Analysis. *Journal of Computational Chemistry* **2004**, 25 (13), 1605–1612. <https://doi.org/10.1002/jcc.20084>.
- (33) Hodoň, J.; Frydrych, I.; Trhlíková, Z.; Pokorný, J.; Borková, L.; Benická, S.; Vlk, M.; Lišková, B.; Kubíčková, A.; Medvedíková, M.; Pisár, M.; Šarek, J.; Das, V.; Ligasová, A.; Koberna, K.; Džubák, P.; Hajdúch, M.; Urban, M. Triterpenoid Pyrazines and Pyridines – Synthesis, Cytotoxicity, Mechanism of Action, Preparation of Prodrugs. *European Journal of Medicinal Chemistry* **2022**, 243, 114777. <https://doi.org/10.1016/j.ejmech.2022.114777>.